Direct-Contact Condensers for ~~Solar Pond Power~~ Production

HEAT EXCH-ANGERS

Elizabeth M. Fisher
John D. Wright

SERI

NOTICE

Direct-Contact Condensers for Solar Pond Power Production

Elizabeth M. Fisher
John D. Wright

May 1984

PREFACE

This report is part of a continuing investigation of the applicability of direct-contact heat exchangers to power production from solar ponds. Earlier work on direct-contact boilers is documented in SERI technical reports TR-631-1122R and TR-252-1401 (Wright 1981, 1982). The present report evaluates the use of direct-contact condensers in a solar pond Rankine cycle.

Approved for

SOLAR ENERGY RESEARCH INSTITUTE

Frank Kreith, Chief
Thermal Research Branch

L. J. Shannon, Manager
Solar Heat Research Division

SUMMARY

Objective

The objective of this report is to explore the possibility of using a direct-contact condenser to reduce the cost of producing electricity from an organic Rankine cycle coupled to a solar pond.

Discussion

Direct-contact heat exchangers are often less expensive than equivalent shell-and-tube heat exchangers because they are more simply constructed and require less material. Heat transfer takes place efficiently as the interface between the two fluids, without an intervening wall. Unfortunately, mass transfer, in addition to heat transfer, may take place in the absence of a dividing wall. The two fluids may contaminate each other during their stay in the heat exchanger.

The system of interest is a power plant in which the working fluid (pentane) is boiled by brine from the storage layer of the solar pond and condensed by brine from the evaporating pond that provides concentrated replacement brine to the solar pond. Three possible direct-contact condenser designs are considered: drop-type, bubble-type, and packed-bed. Simply replacing the shell-and-tube condenser with one of these direct-contact options would result in contamination problems. Air from outside would enter the condenser along with the brine, and pentane would leave the condenser dissolved in the brine and be lost to the atmosphere. In order to reduce these problems, we designed a deaerator and a degasser to treat the brine stream before it enters and after it leaves the condenser, respectively.

Size and cost are estimated for each direct-contact condenser and the accompanying deaerator and degasser. For each piece of equipment, there is a discussion of the correlations or models used for heat and mass transfer, particle terminal velocity, and particle production, as applicable.

Conclusion

The cost of electricity produced using a direct-contact condenser subsystem is estimated to be less than the cost of the electricity produced in a plant with a conventional condenser, for two of the three design options. However, the reduction in cost was not significant enough to compensate for the uncertainties involved in the relatively new technology of direct-contact heat transfer.

TABLE OF CONTENTS

LIST OF FIGURES

LIST OF FIGURES (Concluded)

LIST OF TABLES

NOMENCLATURE

		Units*
A	cross-sectional area of direct-contact condensers, deaerators, and degassers; surface area of shell-and-tube heat exchangers	m^2
A_f	total area of holes in a perforated plate	m^2
A_t	total area of perforated plate (including holes)	m^2
a	specific area of packing	m^2/m^3
a_s	surface area of a tube per unit length	m^2/m
a_w/a_t	ratio of wetted to total area of packing	--
B	ratio of the products of flow rate and specific heat, defined as $\dot{m}_L C_{pL}/(\dot{m}_v C_{pv})$	--
C	cost of cooling tower	$
C_D'	fictitious drag coefficient	--
C_p	specific heat	$J/(kg\ ^oC)$
C_s	cost of fabrication	$
D	diameter	m
D_p	characteristic diameter of packing	m
d	diffusivity	m^2/s
e	efficiency	--
F	packing factor	--
F_1, F_2	costing factors for cooling tower	--
Fo	Fourier number, defined as $k_L t/(\rho_L C_{pL} R_0^2)$	--
f	friction factor	--
g	acceleration due to gravity	m/s^2

* -- in the units column mean that the term is dimensionless.

NOMENCLATURE (Continued)

H	Henry's constant	ppm/atm
HTU	height of transfer unit	m
h	film heat-transfer coefficient	$W/(m^2\,{}^oC)$
h_{fg}	heat of vaporization	J/kg
Ja	Jakob number, defined as $h_{fg}/[C_{pv}(T_{sat} - T_{avg})]$	--
Ja*	modified Jakob number, defined as $\rho_L C_{pL}(T_{sat} - T_\infty)/(h_{fg}\rho_c)$	--
K	conversion factor, equal to 9.8	
k	thermal conductivity	$W/(m\,{}^oC)$
L	length	m
M	number of manholes	--
$\dot{m}$	mass flow rate	kg/s
N	number of nozzles, tubes, or holes	--
Nu	Nusselt number, defined as hD/k	--
n	coefficient in the correlation of Golshani and Chen	
P	pressure	Pa
PL	parasitic losses	W
Pr	Prandtl number, defined as $C_p\mu/k$	--
p	power	W
$\dot{Q}$	rate of heat absorption or rejection	W
R	radius	m
r_f	resistance due to fouling	$m^2\,{}^oC/W$
Re	Reynolds number, defined as $2RV\rho/\mu$	--
S	hourly cost of shop labor or fabrication of columns	\$/hr
St*	modified Stanton number, defined as $U_v A/[\dot{m}_v C_{pv}a\,(a_w/a_t)]$	--
T	temperature	^oC

NOMENCLATURE (Continued)

t	time	s
U_v	volumetric heat transfer coefficient	$W/(m^3 \, {}^oC)$
U_s	overall heat transfer coefficient (for shell-and-tube heat exchangers)	$W/(m^2 \, {}^oC)$
V	velocity	m/s
v	volume	m^3
W	weight of material for a piece of equipment	tons
We	Weber number, defined as $V_{or}^2 D_{or} \rho_v / \sigma_L$	--
X	concentration	ppm
Y	expansion factor for gases passing through orifices	--
Z	height	m
Z'	dimensionless height, defined Z/D_p	--
α	coefficient in the correlation of Golshani and Chen	
μ	viscosity	kg/(ms)
ρ	density	kg/m^3
σ	surface tension	N/m
τ	dimensionless time, defined $k_L t / (\rho_L \, C_{pL} \, R_0^2)$	--
ϕ	effectiveness, defined for a drop-type condenser as the ratio of the thickness of the condensate film to the radius of the drop	--

Subscripts

a	air
avg	average
c	condensate (i.e., pentane liquid)
d	drop
da	deaerator
eq	equilibrium

NOMENCLATURE (Concluded)

i	inner
int	interface
L	liquid (i.e., brine or water)
LM	log mean
l	lateral
o	outer
or	orifice
sat	saturation
T	terminal
t	turbine
v	vapor (i.e., pentane vapor)
0	initial
∞	final or far away from bubble

SECTION 1.0

INTRODUCTION

A solar pond coupled to an organic Rankine cycle power plant converts sunlight first to heat and then to electricity. The difference between the pond storage zone temperature and ambient temperature is small (<100°C) in comparison to the temperature driving force for coal-fired or nuclear power plants. A low driving force implies a low efficiency for Rankine cycles: under typical operating conditions for a solar pond power plant, approximately 90% of the heat removed from the solar pond must be rejected into a cooling pond. For that reason, heat exchangers, usually shell-and-tube, account for a large part of the capital cost of this sort of power plant.

Previous work at SERI has investigated the possibility of replacing the shell-and-tube preheater/boiler with a direct-contact heat exchanger, in which the working fluid bubbles through the hot brine from the solar pond. On the basis of its cycle efficiency and low solubility in brine, Wright (1981) selected pentane as the best working fluid for a Rankine cycle with a direct-contact preheater/boiler. In 1982, he sized the preheater/boiler and found its cost to be about 10% of the cost of an equivalent shell-and-tube heat exchanger (Wright 1982). Figure 1-1 is a diagram of the plant designed by Wright.

This report examines the feasibility of using a direct-contact condenser for solar pond power production in a 5-MWe plant. Wright dismissed the idea in his 1981 report because he found the pentane loss unacceptably high for the system he selected: a condenser cooled with fresh water that flows directly
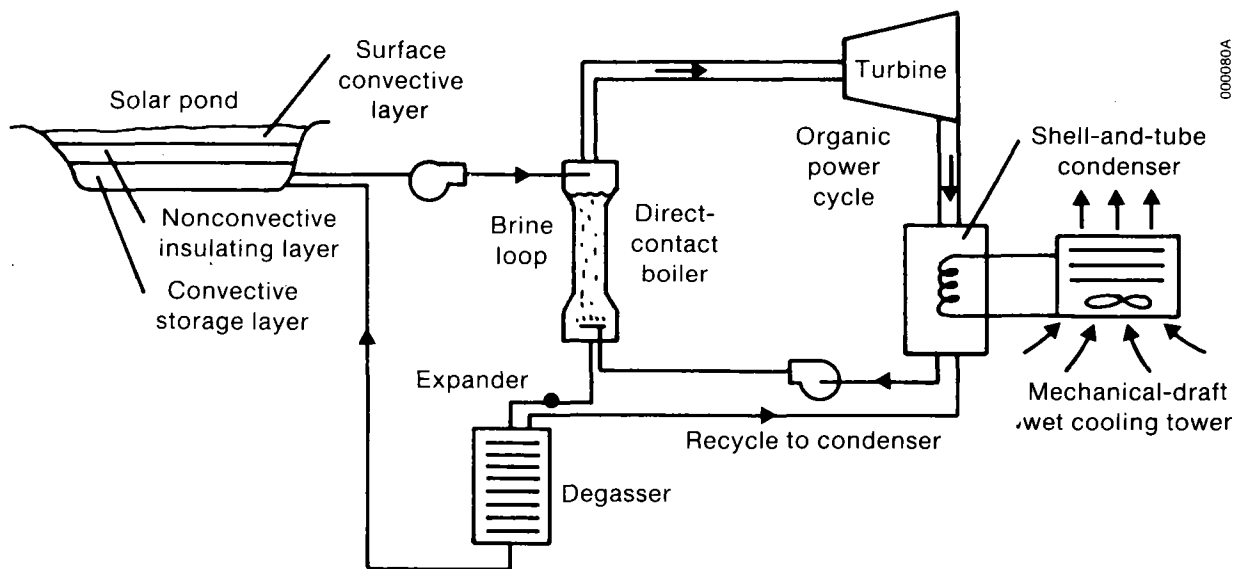
Figure 1-1. Organic Rankine Cycle Coupled to a Solar Pond

to a wet cooling tower. This report considers a different system, which has much smaller working fluid losses for the following reasons: first, concentrated brine, in which pentane has a very low solubility, is used as the coolant, and second, a degasser recovers some of the dissolved pentane. The concentrated brine is obtained from evaporating ponds that are required for solar pond maintenance even if electricity is not produced. In this report, we evaluate three possible direct-contact condenser designs: drop-type, bubble-type, and packed bed, as well as one conventional design. The evaluation is done by sizing and costing the options for a 5-MWe power plant and comparing costs. Section 2.0 describes the components of the system. Section 3.0 explains the method used to compare the different designs. In Sections 4.0 and 5.0, correlations are presented for designing the direct-contact and shell-and-tube condenser subsystems, respectively; Sections 6.0 and 7.0 provide designs and cost estimates. Section 8.0 gives cost estimates for the entire plant for each option. Section 9.0 concludes that, within the accuracy of this analysis, the use of a direct-contact condenser somewhat reduces the cost of power. However, this cost reduction is probably not large enough to compensate for the uncertainties still associated with the new technology of direct-contact condensation.

SECTION 2.0

SYSTEM DESCRIPTION

This section describes the organic Rankine cycle (Section 2.1) and, within it, the components of the condenser systems under consideration (Section 2.2). It also states the performance requirements assumed in this study for each component.

2.1 RANKINE CYCLE

In an organic Rankine cycle, an organic working fluid travels in a loop from boiler to condenser and back again. Between the boiler and the condenser, the fluid does work on a turbine, producing electricity. After the liquid working fluid leaves the condenser, work is done on it to pump it back to boiler pressure. Figure 2-1 shows the components of the working fluid loop. In the system examined in the report, the working fluid is pentane, the heat source is hot brine from the storage layer of a solar pond, and the heat sink is a reservoir of brine or fresh water at atmospheric pressure and near ambient temperature. The boiler is a packed-column direct-contact heat exchanger described in an earlier SERI report (Wright 1982).

Four types of condensers are examined in this report: three direct-contact condensers and one shell-and-tube condenser. In the bubble-type direct-contact condenser, bubbles of pentane vapor condense into drops of pentane liquid as they rise through a continuous phase of brine. In the packed-bed
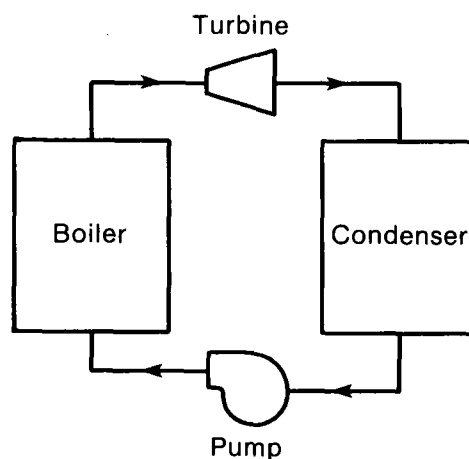
Figure 2-1. Working-Fluid Loop

and drop-type condenser, however, pentane vapor is the continuous phase: in the drop-type condenser, the pentane condenses in a thin film on falling droplets of brine; in the packed-bed condenser, it condenses in a thin film on a layer of brine that flows over packing. The three direct-contact condensers are compared to a conventional shell-and-tube condenser that uses water as a coolant. Water, rather than brine, was selected on the assumption that corrosion problems would be severe if brine were used in a shell-and-tube heat exchanger.

2.2 CONDENSER SUBSYSTEM

Because of the nature of direct-contact heat transfer, the components of the coolant loop for a direct-contact system are different from those of a plant using shell-and-tube heat exchangers. Figures 2-2 and 2-3 show the condenser subsystems for a shell-and-tube condenser and for a direct-contact condenser, respectively. The shell-and-tube subsystem consists of a shell-and-tube heat exchanger and a cooling tower. The direct-contact subsystem consists of a direct-contact heat exchanger, a degasser, a deaerator, and an evaporating pond.

In the shell-and-tube condenser, pentane condenses on the outside of tubes through which cool water is flowing. The pentane must reject enough heat to change from a superheated vapor to a liquid. The water absorbs this heat as it passes through the condenser; it must reject the same amount of heat into the air in the evaporative cooling tower.

Because of air leaks, it is impossible to keep the pentane vapor in the condenser entirely free of noncondensable gases. To maintain the condenser's pressure at the low level required, these gases must be removed from the condenser continuously. Before being vented to the atmosphere, they pass through the vent condenser, shown in Figure 2-2, where some of the pentane carried with them is condensed.

The direct-contact condenser subsystem is more complicated because the pentane and brine can contaminate each other when they come into contact in the condenser. This subsystem still includes a condenser and a vent condenser, which perform the same functions as those in the shell-and-tube system. In addition, it includes a deaerator and a degasser. The coolant is brine from the most concentrated of the evaporating ponds associated with the solar pond, and heat is rejected directly into this evaporating pond, without a cooling tower. The rejected heat speeds up the process of concentrating brine for solar pond maintenance.

Brine is pumped from the evaporating pond through a deaerator before it enters the condenser. The deaerator is necessary in the direct-contact system for three reasons that do not apply to the shell-and-tube system. First, the corrosive effect of brine is greatly reduced when oxygen content is reduced. Second, since the condenser operates at subatmospheric pressure, some air will come out of solution and degrade condenser performance unless the brine is deaerated before it comes into contact with the working fluid. Finally, deaeration reduces the possibility of producing an explosive mixture of oxygen and pentane vapor in the condenser or degasser. A deaerator is needed because

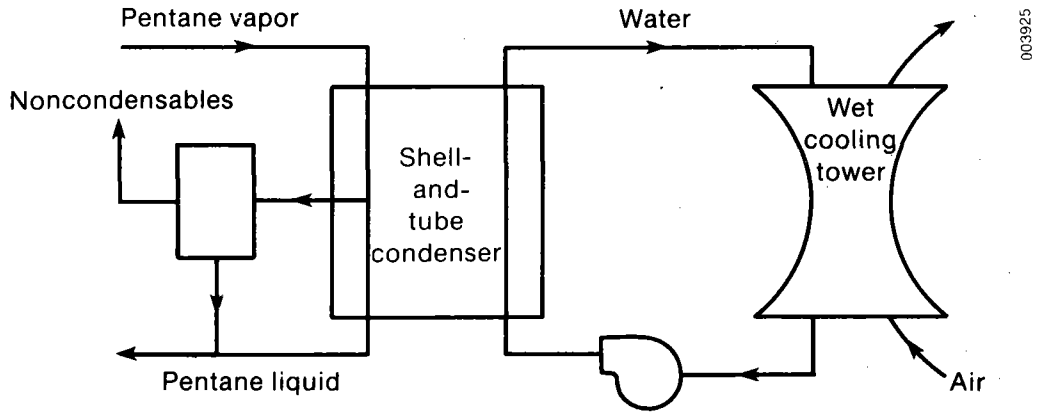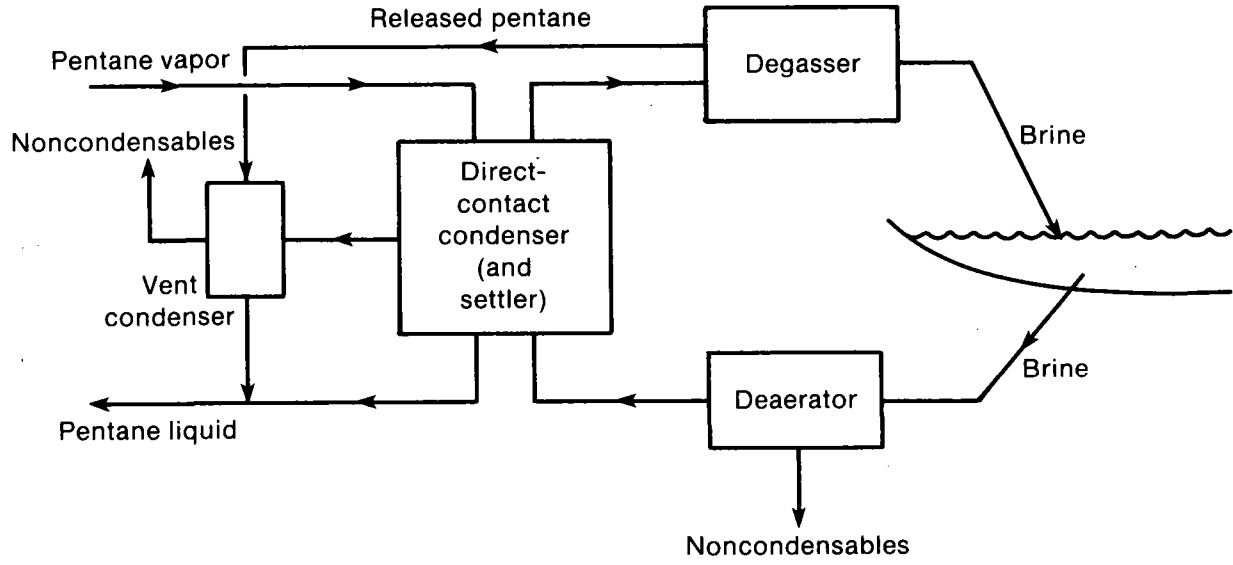**Figure 2-2.   Shell-and-Tube Condenser Subsystem**

Figure 2-3.   Direct-Contact Condenser Subsystem

brine is used as a coolant and a direct-contact condensation process is employed.

We chose deaerator performance requirements on the basis of condenser performance, and found that these requirements were stringent enough to reduce corrosion and explosion problems drastically as well. A small amount of noncondensable gas is present in any subatmospheric condenser, direct-contact or shell-and-tube, because of air leaks. We arbitrarily assumed that this amount would be 1% by volume of the pentane vapor present. A direct-contact condenser without a deaerator may have a considerably larger percentage of noncondensables, for the following reason: according to Henry's law, the equilibrium concentration of air in brine is directly proportional to the partial pressure of air above the brine. If the brine travels directly from the evaporating pond to the condenser, the partial pressure of air, and consequently the equilibrium concentration of air in the brine, are reduced to approximately 1% of their value outside, and air is released. The function of the deaerator is to reduce the concentration of air in the brine so that it will be in equilibrium with the 1% noncondensables in the condenser. Thus, the brine will not release any air in the condenser, and the direct-contact and shell-and-tube condensers will have the same problems with noncondensables.

Removing 99% of the dissolved air reduces corrosion significantly, since the dependence of the corrosion rate of steel on brine oxygen content is approximately linear. Diamant (1971) and Schumacher (1979) plot corrosion rate versus oxygen content for dilute salt solutions. We can use these data as estimates of corrosion rates for concentrated brine. Extrapolated from data on solubility at high pressures in the Saline Water Conversion Engineering Data Book (M. W. Kellogg Company 1975), the concentration of oxygen in 25% brine at one atmosphere total pressure is 0.9 ppm (parts per million, by weight). The deaerator will reduce that concentration to less than 0.009 ppm. This reduces the corrosion rate for dilute brine from 0.08 to 0.02 mm of steel per year, or from 2.3 mm to 0.6 mm over the 30-year lifetime of the plant.

According to Sax (1979), pentane vapor and air can form an explosive mixture if the fraction of pentane is between 1.5% and 7.8%. So, the likelihood of producing an explosive mixture is very small in the condenser, where there is far more pentane vapor then air, or in the degasser, where more than 100 times as much pentane as air is present in the brine. The likelihood becomes even smaller when the deaerator is introduced.

Henry's law governs the absorption of pentane as well as the desorption of air in the condenser. It is conservative to assume that the brine will become saturated with pentane during its residence in the condenser, and that any pentane that enters the evaporating pond with the brine will be desorbed and lost into the atmosphere. Although pentane is much less soluble in concentrated brine than in fresh water (Hellstrom, Jacobs, and Boehm 1976; see Figure 2-4), it is not economically feasible to lose as much pentane as can be dissolved in brine at the condenser pressure. This would result in a pentane replacement cost of over two million dollars during the lifetime of the plant, the same order of magnitude as the cost of a shell-and-tube condenser. For that reason, a degasser must be inserted between the condenser and the
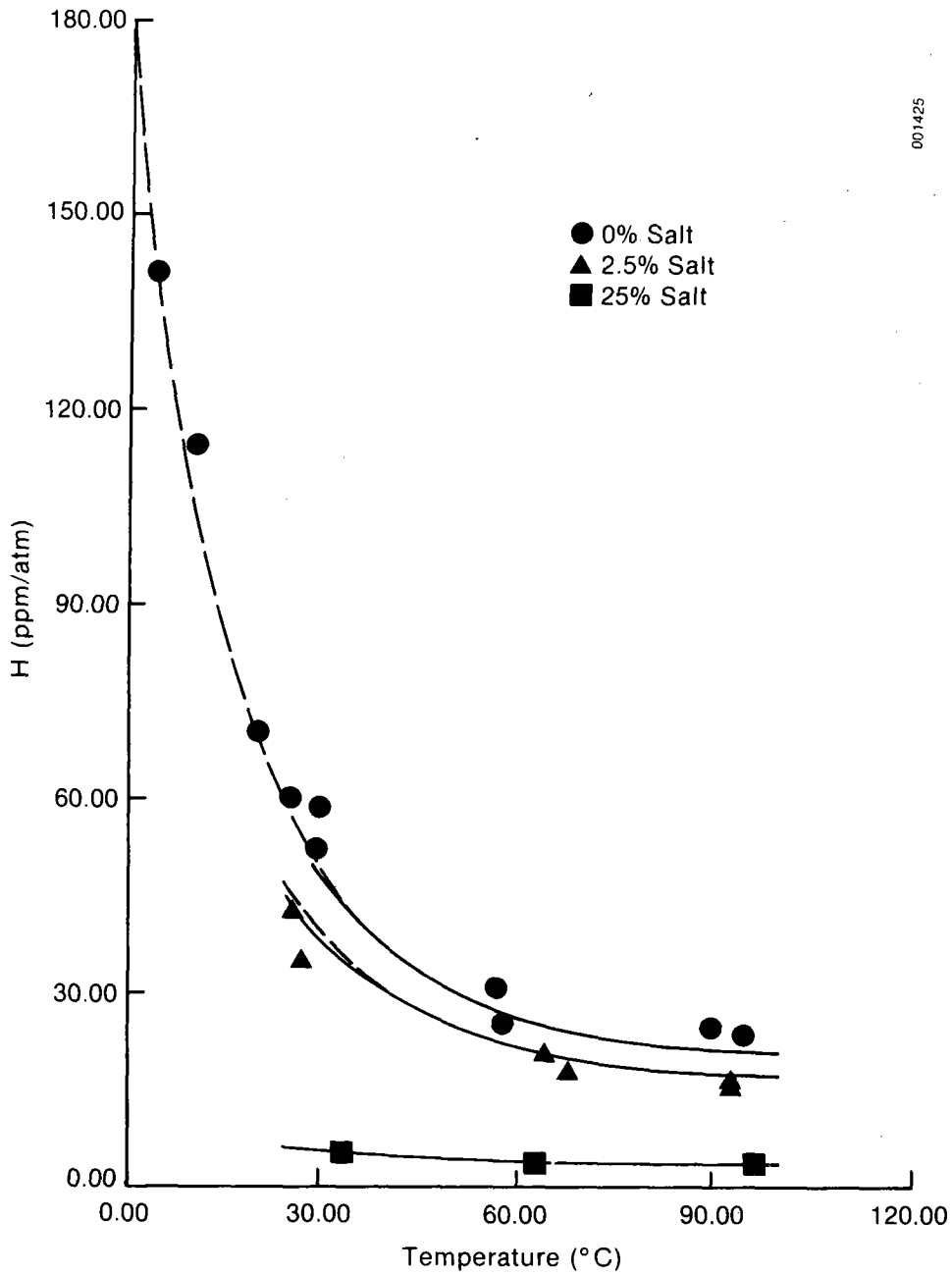
Figure 2-4. Solubility of Pentane in Aqueous Saline Solutions

evaporating pond to retrieve some of the dissolved pentane. The degasser releases pentane vapor, which can be sent either to the main condenser or the vent condenser. For simplicity in the analysis, we chose to return it to the main condenser. Condenser performance is impaired when water vapor and air are returned to the condenser along with the pentane, but we neglected the impairment because the water vapor is condensable and the amount of air is very small.

The degasser must be designed to remove all but a certain amount of pentane from the brine stream. One way to determine the design requirements is to find the minimum of the sum of the degasser cost and the present worth of pentane lost over the lifetime of the plant. A more stringent condition on degasser performance, based on safety, was used in this analysis. If the air above the surface of the evaporating pond is stagnant, the partial pressure of pentane, and thus the concentration of pentane in the layer of air nearest the surface, is related to the concentration of pentane in the brine by Henry's law. Thus, the degasser duty was determined by requiring that the pentane concentration in the air above the evaporating pond be below the lower explosive limit. This requirement is probably stricter than necessary, since convection currents normally present over a cooling pond will disperse the pentane vapor quickly. The safety requirement reduces the cost of pentane lost to a small percentage of the plant's operating expenses.

SECTION 3.0

METHOD OF COMPARISON

This section describes how we compared the four condensers mentioned earlier, which exhibit different vapor-side pressure drops and brine-side parasitic losses. The fairest way to choose among the four options would be to optimize each condenser subsystem on the basis of cost per net electrical output over a typical year and compare these costs. Time constraints, however, necessitated the use of a simpler, somewhat arbitrary, comparison procedure: we sized the four condenser subsystems so that the plants that they belong to produce the same gross amount of electricity under the same conditions. Section 3.1 specifies these conditions. Then, we compensated for the subsystems' different parasitic losses. We computed the efficiency of each entire power plant and increased the size of each power plant to produce 5 MW$_e$ net. The final comparison is based on the cost of these scaled-up plants. Section 3.2 gives the details of the scale-up and costing process. If there is a substantial cost difference between one of the direct-contact subsystems and the shell-and-tube subsystem, this procedure should be sufficient to detect it. If the difference is not large, then this technique and optimization may give conflicting results. However, because of the many uncertainties associated with direct-contact design, the direct-contact subsystem will be competitive only if it is much less expensive than the conventional shell-and-tube subsystem.

Before scale-up, the condenser subsystem is sized for the power plant described in Wright's earlier reports (1981, 1982) and shown in Figure 1-1. Wright designed the plant, which has a direct-contact boiler and a shell-and-tube condenser, for a net power output of 5 MW$_e$. However, this design neglected the parasitic losses of the condenser subsystem. So, in each case, it is necessary to enlarge the entire plant to produce 5 MW$_e$ net after sizing the condenser subsystem for compatibility with Wright's original plant design. Wright's early cost estimates for plant components outside of the condenser system will be used in the scale-up and costing process described here.

3.1 DESIGN CONDITIONS AND ASSUMPTIONS

In the first stage of the design procedure described above, all of the condenser subsystems under consideration must fit into plants that have the same gross power output. This is achieved by requiring the same mass flow rate of pentane (115 kg/s) and turbine exit pressure (73.8 kPa) for all designs. The constraint on turbine exit pressure implies that the condensers have the same pressure at the pentane inlet. However, the pressure at which condensation occurs (taken as the average pressure inside the condenser) is different for the different designs. For example, pentane vapor remains at approximately the same pressure throughout the drop-type condenser, in which it is the continuous phase. On the other hand, the vapor in the bubble-type condenser experiences a significant pressure drop as it passes through the orifice plate and rises as bubbles through the brine. There is a penalty for condensers that have large pressure drops: lowering the condenser pressure lowers the saturation temperature of the pentane and thus decreases the driving force for

condensation. This decrease in driving force must be counterbalanced by an increase in area of contact or residence time, and thus by an increase in condenser size and cost.

Aside from the requirements for pentane flow rate and inlet pressure, the main constraints on the condenser subsystem design involve the coolant loop. We assumed that the coolant is available at 20°C, and chose coolant flow rates to give a reasonable pinch-point temperature difference in the condenser. The saturation temperature corresponding to the turbine exit pressure specified above is 300 K, or 26.85°C, but the temperature at which condensation actually occurs may be lower, as explained in the previous paragraph, by as much as 1°C. To provide a minimum temperature difference on the order of 1°C, we selected 25°C as the coolant condenser exit temperature. For the three direct-contact designs, the coolant is assumed to be brine that is 25% sodium chloride by weight. The brine mass flow rate is 2676 kg/s. The shell-and-tube condenser uses fresh water, which has a higher specific heat than brine. Consequently, it has a lower coolant mass flow rate, 2110 kg/s.

Another factor in condenser design is the amount of noncondensable gases present. Section 2.2 describes how we assumed that 1% of the gases in the condenser would be noncondensable gases because of leaks, and then demanded that the deaerator prevent any other noncondensables from entering. This condition was used in the deaerator design, but not in the condenser design, because the effects of noncondensables on condenser performance are known for only some of the condenser options under consideration. In order to evaluate all four condenser types, we designed the condensers themselves assuming that there were no noncondensables.

A final simplifying assumption involves the desuperheating duty of the condenser. According to Wright's 1981 design, pentane vapor should leave the boiler superheated by 5°C. So the vapor must be desuperheated before it can be condensed. The desuperheating load is 28 kJ/kg pentane, or less than 10% of the condensing load. To simplify the problem, we assumed that sensible heat transfer takes place at the same rate as condensation for the systems under consideration. In sizing the condensers, we replaced the heat of vaporization, h_{fg}, with a pseudo-h_{fg} equal to the sum of the heat of vaporization and the desuperheating load per kilogram of pentane.

3.2 SCALE-UP AND COSTING PROCEDURE

Using the assumptions described in the preceding subsection and the heat transfer and flooding relations given in Sections 4.0 and 5.0, we sized each condenser subsystem. We then calculated the parasitic losses associated with each condenser subsystem ($PL_{condenser}$). Knowing this quantity, as well as the heat absorbed and rejected by the power plant (Q_{in} and Q_{out}, respectively) the parasitic losses of the rest of the plant (PL_{other}) and the turbine efficiency, e_t, we were able to calculate the overall thermodynamic efficiency of the plant, e_i, for each design as follows:

$$e_i = \frac{work_{out,i}}{heat_{in}} = \frac{e_t(Q_{in} - Q_{out}) - PL_{other} - PL_{condenser,i}}{Q_{in}} .$$

When the entire plant is enlarged, the efficiency should remain nearly constant for the following reasons: first, as long as pressures and temperatures are kept constant, Q_{in} and Q_{out} are directly proportional to the mass flow rate of the working fluid. The main parasitic losses, too, are proportional to pentane mass flow rate. In the condenser subsystem, the most important parasitics (described in detail in Section 6.0) are proportional to the coolant flow rate, which, in turn, is proportional to the working fluid flow rate. In the rest of the plant, the major parasitics are the work of pumping the working fluid from condenser to boiler and the work of pumping hot brine from the storage layer of the solar pond to the boiler. Both of these are proportional to working fluid flow rate. Thus, since the most important parts of both the numerator and the denominator are directly proportional to working fluid mass flow rate, the system efficiency is practically independent of the size of the plant.

The fact that the efficiency can be taken as constant for each of the condenser types makes the scale-up process fairly simple. Using the efficiency for each plant, we calculated the amount of heat the working fluid must absorb (Q_{in}) in order to produce a given net power output (5 MW$_e$) as follows:

$$Q_{in,i} = (5 \text{ MW}_e)/e_i \ .$$

From the heat requirements, we calculated the working fluid and coolant mass flow rates for a 5-MW$_e$ plant. We resized the condenser subsystem and costed it by the method developed by Pikulik and Diaz (1979), described in Section 6.0. Wright used the same method in his 1982 report.

For a fair cost comparison, it is necessary to include the cost of the rest of the plant and of the solar pond scaled for the new flow rate. Instead of resizing the entire plant, we applied the empirical "six-tenths rule" (Peters and Timmerhaus 1968) to the cost estimates provided by Wright (1981, 1982) for the components of the plant other than the condenser subsystem. According to this rule, the ratio of the costs of two similar pieces of equipment is roughly equal to the ratio of their capacities raised to the six-tenths power. For the solar pond itself, we assumed that the cost is linearly dependent on the amount of heat removed. The cost of the evaporating pond depends on the weather conditions at the site and on the amount of heat rejected into it by the condenser. Thus, an evaporating pond associated with any of the direct-contact condensers will be less expensive than one associated with a power plant that rejects heat into a cooling tower. However, this cost difference is neglected because the cost of the entire evaporating pond is a fairly small part of the cost of the entire system.

SECTION 4.0

RELATIONSHIPS USED IN SIZING DIRECT-CONTACT
CONDENSER SUBSYSTEMS

In this section, we present the experimental correlations and the-oretical relationships used to size the components of the direct-contact subsystems: the three condensers, the deaerator, and the degasser. We also explain how each component's parasitic losses are calculated. The section is arranged component by component.

4.1 DROP-TYPE CONDENSER

A schematic of the drop condensation process is shown in Figure 4-1. The brine stream passes through nozzles and enters the condenser as a spray of droplets. The pentane vapor from the turbine enters the condenser from the side and forms the con-tinuous phase around the drops. Pentane vapor condenses on the drops and the coolant and condensate collect at the bottom of the condenser. From there, they travel to a settling tank, where the buoyant pentane liquid rises from the brine.

Figure 4-1. Schematic Drawing of a Drop-Type Condenser

The size of the condenser is determined as follows: heat transfer relation-ships described in Section 4.1.1 specify the residence time required of the brine as a function of droplet radius and other condenser conditions. The residence time requirement can be converted to a height requirement using noz-zle exit velocities and terminal velocity correlations. This procedure is described in Section 4.1.2. The cross-sectional area of the condenser is chosen on the basis of nozzle spacing. An average drop size can be predicted for given nozzles and pressure drops using information supplied by the spray nozzle manufacturer. Drop size and condenser area are chosen in Section 6.1, in which the drop-type condenser is designed.

This condenser has the advantage of a low vapor-side pressure drop. For this analysis, condensation is taken to occur at the turbine exit pressure, with no pressure drop. The disadvantage of this choice of condenser lies in the high parasitic losses associated with it. The brine has a large, nonrecoverable head loss as it passes through the nozzles and as it falls through the pentane vapor. Another problem is that the brine and pentane must be separated after they leave the condenser.

4.1.1 Heat Transfer in Drop-Type Condenser

The heat transfer relationships selected for this analysis were developed by Jacobs and Cook (1978), using a theoretical model of a single, noncirculating drop. Their model is more applicable to the system under consideration than most of the literature on barometric condensers because it takes into account the resistance to heat transfer of the film of condensate surrounding the drop. Most other published papers are concerned with the condensation of steam on water, for which condensate resistance is much less important.

Jacobs and Cook derive a relationship between drop radius and residence time as follows: first, they assume that the only form of heat transfer within the drop is conduction, and that the condensation rate is controlled by the liquid side. Then, they simplify the problem by neglecting the thermal capacitance of the condensate and assuming that the condensate film has a linear temperature profile. These simplifications are valid when the film of condensate is thin. This leaves them to solve a simplified energy balance and the conduction equation for the coolant drop. They perform a numerical solution and present their results in graphs, such as Figure 4-2, of dimensionless drop residence time required for a given degree of utilization of the coolant as a function of temperature driving force. An index of the degree of coolant utilization is the effectiveness, ϕ, defined by Jacobs and Cook as the ratio of condensate thickness on the drops at the bottom of the condenser to the maximum thickness attainable with the temperature driving force available. Results of the numerical solution are provided for $\phi = 0.5$ and $\phi = 0.75$. We selected the higher utilization of the coolant, $\phi = 0.75$. Figure 4-2 shows the residence time requirement as a function of temperature driving force, in terms of τ, the dimensionless time, which is defined as $k_L t/(R_0^2 \rho_L C_{pL})$.
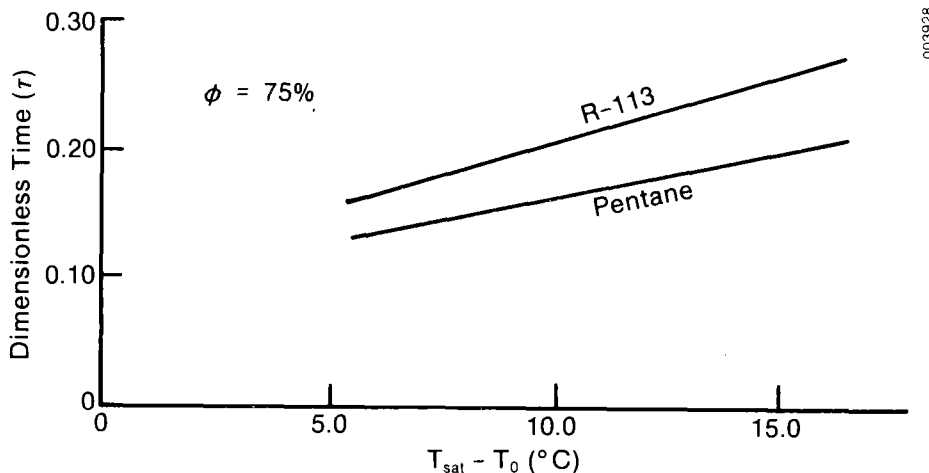
Source: Jacobs and Cook 1978

Figure 4-2. Dimensionless Drop Residence Time Required for 75% Effectiveness
Source: Jacobs and Cook 1978.

13

Figure 4-3 is derived from the information in Figure 4-2 about the conditions under which the condenser will operate. It gives the residence time requirement in terms of drop size.

Jacobs (1984) recommends that this heat transfer relationship be combined with information about the distribution of droplet sizes from the nozzle for design purposes. For a preliminary design, he advises that the design be based on the largest drop size produced by the nozzle, because a large drop contributes more to condensation than a small one. Since the information provided by the spray nozzle manufacturer gives the mean drop radius, and not a maximum or size distribution, we used twice the median radius in our design.

There is some inaccuracy involved in applying Jacobs and Cook's model to the analysis of a drop-type condenser. The model treats drops as rigid, noncirculating spheres, an approximation that is accurate only for very small drops. According to Clift, Grace, and Weber (1978, p. 178), only drops smaller than 400 microns should be treated as rigid spheres. Because the production of small drops entails a substantial energy loss, it is not feasible to design the condenser with drops in the rigid sphere range. Larger drops are likely to have internal circulation and a nonspherical shape, with a larger surface area. Since both of these phenomena should enhance heat transfer, the rigid, noncirculating sphere assumption is a conservative one.

The other main difference between the model and the real system under consideration concerns drop interactions. Jacobs and Cook analyze a single drop falling freely through vapor; in a real condenser, drops collide and interact with each other in other ways. Collisions could either improve or worsen the overall heat transfer rate. Collisions enhance heat transfer because they
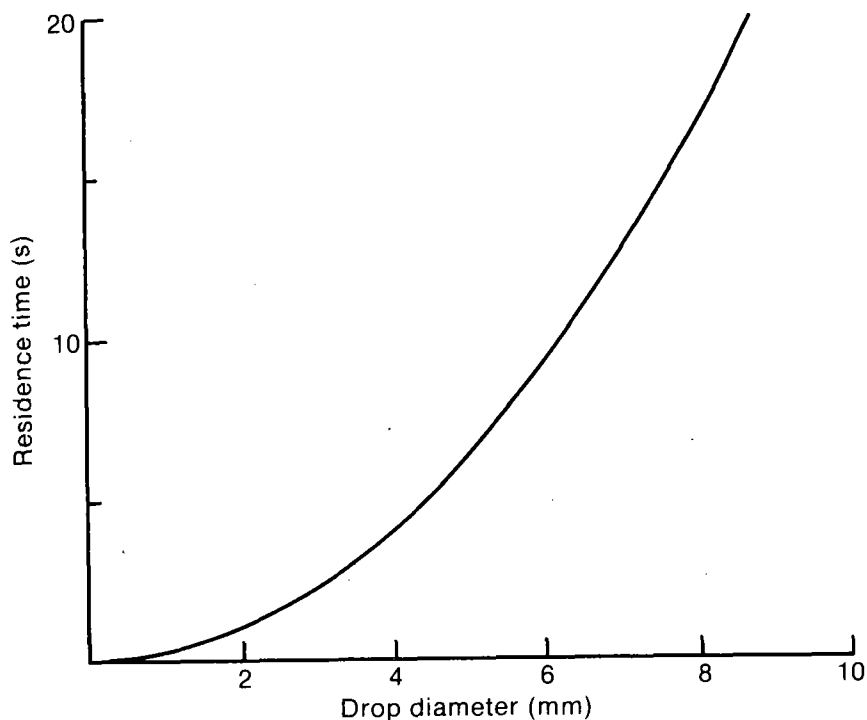
Figure 4-3. Drop Residence Time versus Drop Diameter

promote circulation within drops and because they sometimes result in an increase of surface area. However, some collisions end in the coalescence of the colliding drops, decreasing the surface area available for heat trans-fer. In addition, drops affect each other's velocity even when they do not collide. An ensemble of drops falls at a "hindered velocity" which is slower than the terminal velocity of a single drop. This increases the time avail-able for heat transfer in a given height, but it also implies that the vapor undergoes a measurable pressure drop. Finally, the presence of an ensemble of drops may hinder heat transfer. As they fall, some drops will be partially shielded by others from pentane vapor. Thus, the heat transfer process may be controlled by the availability of vapor rather than by the conduction rate through the drop. Because of this variety of effects, it is not clear whether the single drop assumption is conservative or optimistic.

4.1.2 Drop Velocity

The height of a drop-type condenser is determined using heat transfer rela-tionships (Section 4.1.1) and knowledge of the drops' velocities. For termi-nal velocities of liquid drops falling in gases, Clift, Grace, and Weber (1978, p. 179) recommend the correlation of Garner and Lihou, based on experi-mental data on liquid drops in air. Drop interactions and wall effects are negligible in the experiments used for their correlation, shown in dimensional form in Figure 4-4. Since the drops may leave the spray nozzle with a velocity greater than terminal, the time available for heat transfer may be shorter than that predicted by using the terminal velocity correlation throughout the fall of the drop. The deceleration of a drop can be calculated from the drag coefficient, but correlations are not available for the drag
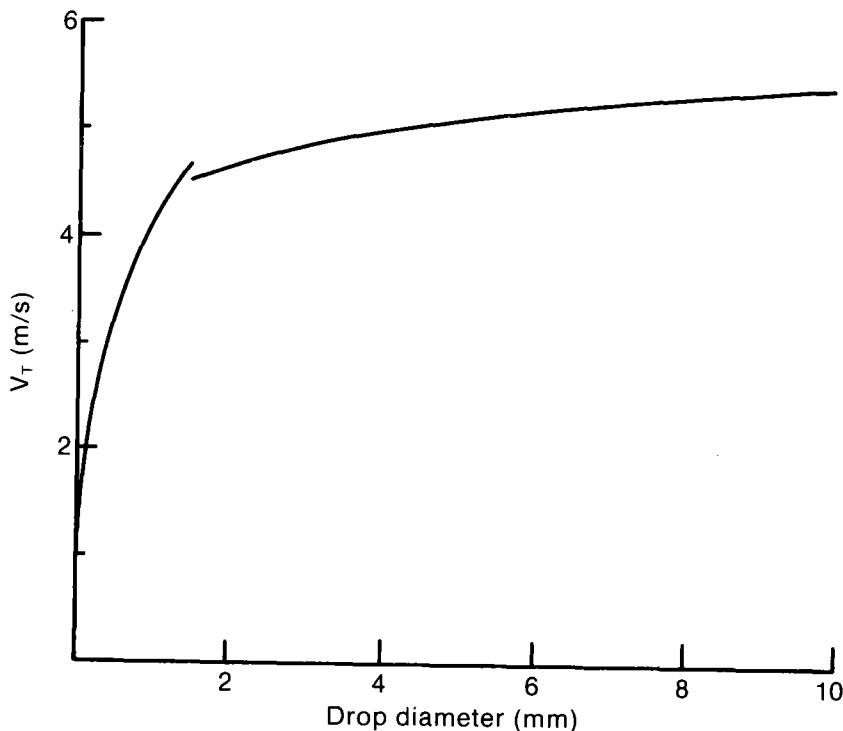
Figure 4-4. Terminal Velocity of Drops

coefficient of a liquid drop in a gas. In order to approximate the deceleration, we used the terminal velocity correlation of Garner and Lihou to create a fictitious drag coefficient as follows. We computed the drag coefficient required to balance gravitational and drag forces at terminal velocity V_T, using the equation

$$\frac{4}{3} \pi R_d^3 g \left[\rho_L - \rho_v \right] = \frac{C_D'}{2} \rho_v V_T^2 \pi R_d^2 \, ,$$

where R_d is the drop radius (m), g is the acceleration due to gravity (m/s^2), ρ_L is the density of the brine (kg/m^3), ρ_v is the density of the pentane vapor (kg/m^3), C_D' is the fictitious drag coefficient (dimensionless), and V_T is the terminal velocity (m/s). We assumed that the drag coefficient derived from this expression, $C_D' = (8/3)g(\rho_L - \rho_v)R_d/(\rho_v V_T^2)$, was valid through the entire fall of the drop, and not just at terminal velocity. With this assumption, a force balance leads to a differential equation easily integrated to give the following expression for the height a drop has fallen as a function of time:

$$dz = Vdt = VdV / \left(g \left[\frac{\rho_L - \rho_v}{\rho_L} \right] - \frac{3}{8} \left[\frac{\rho_v}{\rho_L} \right] \frac{C_D'}{R_d} V^2 \right) .$$

This expression is used to calculate the condenser height needed for a given drop residence time. The drag coefficient is evaluated with R_d equal to twice the median drop radius for the reasons described in the preceding section. No allowance is made for the increase in drop size due to condensate accumulation, which should change the radius by 10% or less.

4.2 BUBBLE-TYPE CONDENSER

The bubble-type condenser, shown schematically in Figure 4-5, works as follows: Brine enters the condenser on one side near the top and flows out the other side, near the bottom. Pentane enters a chamber below the brine and then passes through the holes of a sieve tray, forming bubbles in the brine. The bubbles condense as they rise. They become drops of pentane liquid, which collect in a layer on the top of the brine. This layer leaves the condenser through its own outlet and is pumped to boiler pressure.

The sizing procedure for the bubble-type condenser is similar to that for the drop-type condenser. Heat transfer and bubble velocity relationships, described in Sections 4.2.1 and 4.2.2, determine the condenser height required for heat transfer. The cross-sectional area is chosen to prevent flooding. That process is discussed in Section 4.2.3. The correlation used to predict bubble size is presented in Section 4.2.4.

The bubble-type condenser has the lowest parasitic losses of the three designs. Because the brine is the continuous phase, the gravitational potential energy that it loses in moving downward in the condenser is recovered in the form of increased pressure. This design is preferable to the other two with respect to liquid separation as well. The pentane separates from the brine in the condensation process, removing the need for a settling

003931
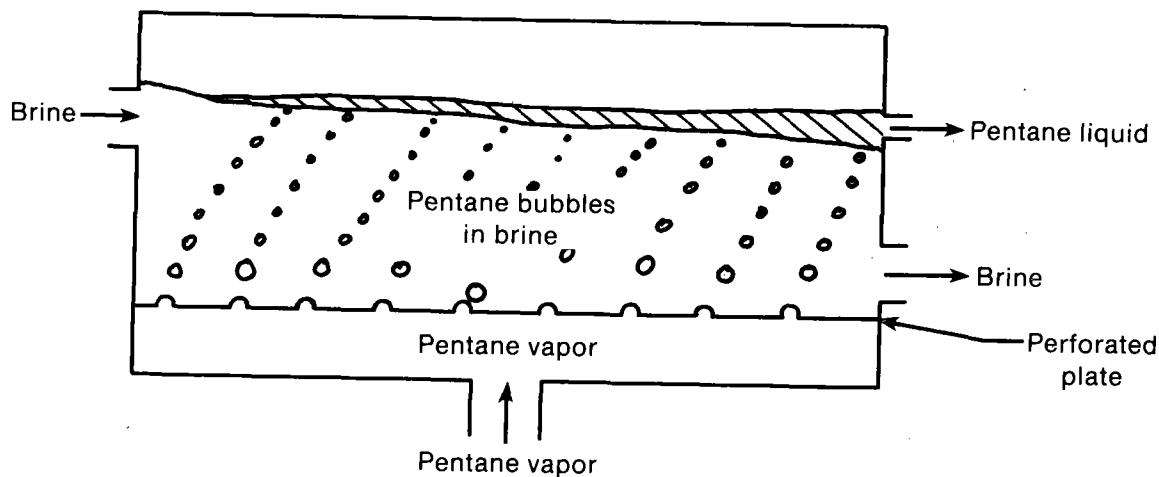
Figure 4-5. Schematic Drawing of a Bubble-Type Condenser

tank. The disadvantage of the bubble-type condenser is that it has a high vapor-side pressure drop. Pentane must overcome both the pressure drop across the orifice plate and the hydrostatic pressure of the brine above. Since all three designs are compared on the basis of constant turbine exit pressure, the high pressure drop has the effect of decreasing the driving force for condensation and thus increasing the height of this particular condenser. This, in turn, increases the pressure drop, so the process of determining condenser height is iterative. As bubble size increases, so does the height of the column of brine required for condensation. For bubbles larger than a certain size, it is impossible to maintain the turbine exit pressure at the desired level and at the same time achieve complete condensation. For that reason the condenser must be designed with small bubbles.

4.2.1 Heat Transfer in Bubble-Type Condenser

The considerable literature on condensation of vapor bubbles is reviewed in a recent article on direct-contact condensation by Sideman and Moalem-Maron (1982). Much of the article concerns the series of papers on bubble collapse, both theoretical and experimental, published by Sideman, Moalem-Maron, Isenberg, and coworkers. The earlier articles in this series concern the collapse of a single bubble of vapor in an expanse of liquid at a uniform temperature. Later articles analyze the collapse of a train of bubbles and of several trains of bubbles taking into account the presence and distribution of noncondensable gases. Most of these studies involve numerical solutions, but approximate analytical solutions are presented for the condensation of a single bubble in motion and for a single train of bubbles. More recent work on bubble collapse includes the derivation of an analytical expression for the

single-bubble case by Jacobs, Fannar, and Beggs (1978) that considers the thermal resistance of the condensate inside the bubble. This resistance is important to the case under consideration because pentane liquid has low thermal conductivity.

Sideman and Moalem-Maron point out that the multi-bubble models predict a slower collapse rate than the single-bubble models for the following reason: the presence of other bubbles makes the water warmer around a given bubble, reducing the driving force for condensation. We chose to use the single-bubble model for ease of analysis, but compensated for the effects of other bubbles by using the average brine temperature, not the cooler inlet brine temperature, to compute the driving force.

We specifically chose the single-bubble collapse model of Jacobs, Fannar, and Beggs, shown in Figure 4-6. The model consists of a vapor bubble surrounded by a film of condensate and then by a thermal boundary layer, the thicknesses of which may change with time. A parabolic temperature distribution is assumed in the boundary layer, and a linear one is assumed in the condensate film. As we mentioned in Section 3.1, noncondensables are assumed to be absent from the condenser. In order to satisfy a no-slip condition at the boundary between the brine and the condensate, the velocity at which the condensate drains to the bottom of the bubble is taken to be equal to the tangential component of the brine's velocity relative to the bubble. The problem of solving an overall energy balance equation for the bubble is simplified by the assumption that the pool of condensate is negligibly small, an assumption that results in only a small inaccuracy until the bubble is 95% condensed.
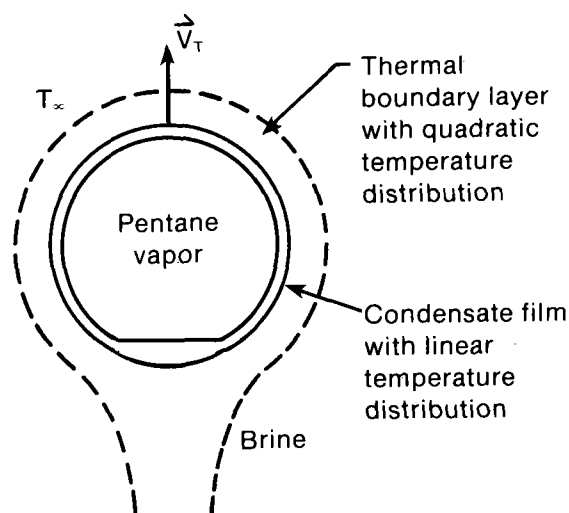
Figure 4-6.   Condensation of a Bubble

Making all these assumptions, Jacobs, Fannar, and Beggs arrive at the following expression for bubble radius as a function of time:

$$\frac{R}{R_o} = \left(1 - 0.6049 \lceil Re_{LO} \, Pr_L \rceil^{1/2} \frac{T_{int} - T_\infty}{T_{sat} - T_\infty} Ja^* \frac{\rho_c - \rho_v}{\rho_v} Fo\right)^{2/3}$$

In this expression, R is the instantaneous radius of the bubble (m), and R_o is the initial radius of the bubble (m). Re_{LO} is the Reynolds number, defined as $2R_o V \rho_L / \mu_L$, where V is bubble velocity (m/s), ρ_L is brine density (kg/m³), and μ_L is brine viscosity (kg/ms). Pr_L is the Prandtl number, defined as $C_{pL} \mu_L / k_L$, where C_{pL} is the heat capacity of the brine and k_L is the thermal conductivity of the brine. T_{int} is the temperature at the interface between the condensate and the brine. T_{sat} is the saturation temperature of the pentane vapor, and T_∞ is the temperature of the bulk liquid surrounding the bubbles. Fo is the Fourier number, defined as $k_L t / (\rho_L C_{pL} R_o^2)$, where t is the time elapsed from bubble formation; ρ_c is the density of the pentane liquid (kg/m³); and ρ_v is the density of the pentane vapor (kg/m³). Ja^* is the modified Jakob number, defined as $\rho_L C_{pL} (T_{sat} - T_\infty) / (\rho_c h_{fg})$.

This equation has the same form as the one derived by Isenberg, Moalem, and Sideman (1970), who neglected the condensate resistance. Both are shown for comparison in Figure 4-7 in dimensional form. The model of Jacobs et al. predicts a faster collapse than that of Isenberg et al. However, both models predict an extremely quick collapse for the bubble size under consideration. Section 6.1.2 shows that, in order to prevent flooding, the bubble-type condenser height must be much greater than either of these heat transfer correlations require.
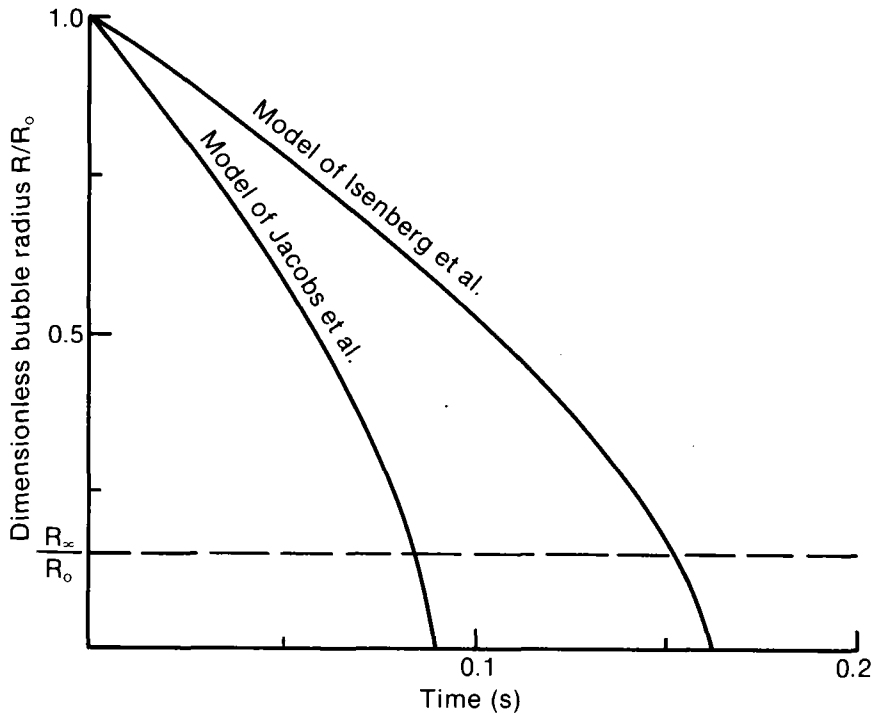
Figure 4-7. Bubble Collapse

Both models shown in Figure 4-7 are most valid for the early stages of collapse, and show physically impossible behavior for later collapse. They show the radius of the bubble decreasing to zero, although a pentane bubble condensing in an immiscible liquid can become no smaller than a liquid drop containing the same amount of pentane. That limit is represented by the horizontal line R_∞/R_0 in Figure 4-7, below which the predictions of the two models should be ignored.

This model has not been directly confirmed by experiments, since the effect of noncondensable gases is significant in all reported experiments. However, when the model is expanded to account for noncondensables (Jacobs and Major 1982), it agrees very well with experimental results.

4.2.2 Bubble Velocity

The problem of making a theoretical prediction of the rise velocity of a condensing bubble is a difficult one, since both the size and the density of the bubble are changing constantly. Furthermore, the problem is coupled to the heat transfer problem described earlier. Fortunately, experiments indicate an approximately constant bubble rise velocity, at least for pentane bubbles with initial radii between 2 and 4 mm, rising in water (Jacobs and Major 1982). The experiments cited study the condensation of a single bubble; it is not known whether multiple trains of bubbles behave the same way. However, it is reasonable to expect the presence of other bubbles to slow bubble rise rather than hasten it.

In this analysis, we assumed that a bubble rises constantly at the terminal velocity associated with its initial properties. Clift, Grace, and Weber (1978, p. 175) review the literature on terminal velocities of drops and bubbles and recommend a correlation from Grace, Wairegi, and Nguyen for systems that are not exceptionally pure. That correlation is shown in dimensional form for the pentane-brine system in Figure 4-8, and is based on a large body of data.

4.2.3 Flooding

The cross-sectional area and height of the bubble-type condenser must be large enough to keep flooding from occurring. Flooding takes place in a two-phase device in one of two ways, depending on the relative flow rates of the two phases. First, if the discontinuous-phase (i.e., pentane) flow rate is high, then particles of the discontinuous phase may crowd together and become the continuous phase. Then, if the continuous-phase (i.e., brine) flow rate is high, then its superficial velocity may be high enough to entrain particles of the discontinuous phase. (The superficial velocity is the velocity at which the continuous phase would travel in an empty column.) We designed the condenser to avoid both of these forms of flooding.

The first form of flooding should be avoided because it would change the geometry drastically and render the heat-transfer relationships derived above invalid. To prevent this, it is necessary to set a condition on the spacing of the bubbles when they are largest; i.e., as they leave the orifice plate.
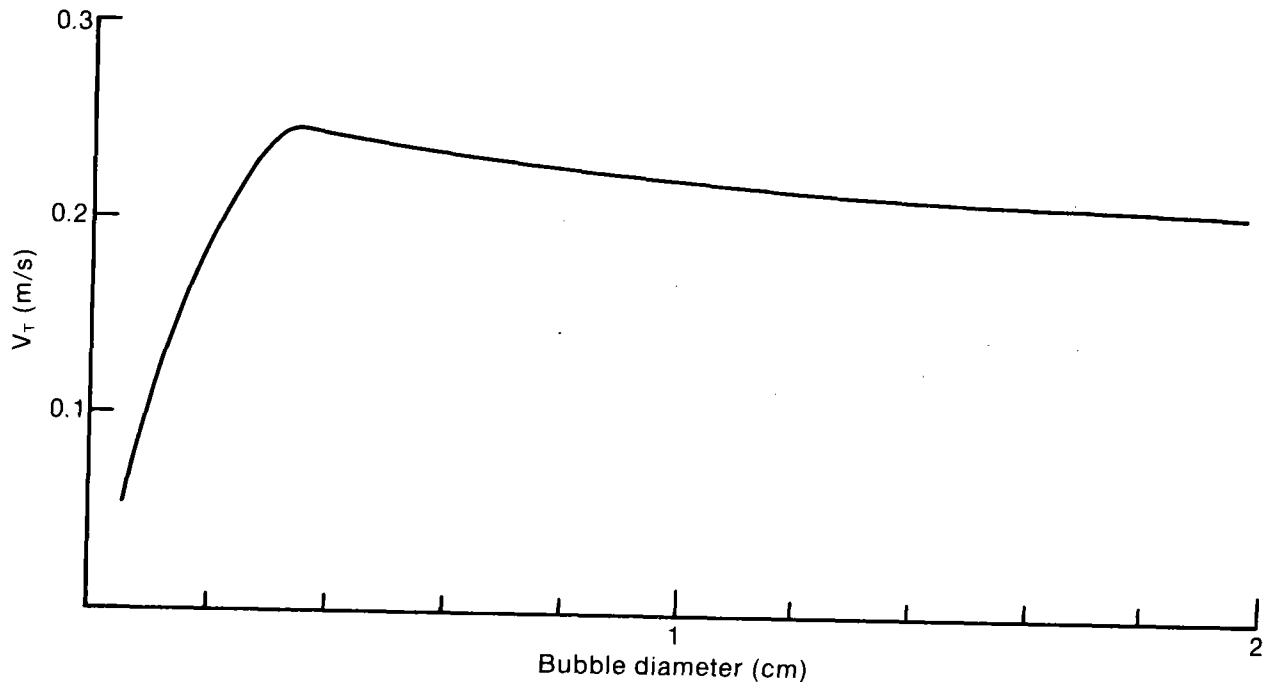
Figure 4-8. Terminal Velocity of Bubbles

We required that the distance between holes in the orifice plate be at least twice the initial radius of a bubble. (At twice the initial radius, bubbles barely touch as they form.) There is still some danger that consecutive bubbles from the same orifice may crowd together and combine. For this reason, the cross-sectional area selected here should be regarded as a lower limit.

The danger of the second form of flooding lies in the fact that a significant amount of pentane will leave the condenser through the exit provided for the brine. It is important to avoid this increase in working fluid loss. If the pentane bubbles rise with a velocity V_T (see Section 4.2.2) through a height Z, and the brine has a lateral velocity V_1 at its exit, then any pentane bubbles formed within a radius of $V_1 Z/V_T$ of the brine exit will be entrained. This means that the portion of the condenser within this radius cannot be used. If the brine velocity is high, then this can be a substantial portion of the cross-sectional area. For a given condenser cross-sectional area, chosen to avoid the first type of flooding, the brine velocity can be reduced by increasing the height of the column of water or by providing more than one brine inlet and outlet orifice.

4.2.4 Bubble Formation

The problem of predicting bubble size has received extensive treatment in the literature, both theoretical and experimental. Mersmann (1978) summarizes recent results about bubble formation and presents them in a nomograph for convenience. The nomograph, shown in Figure 4-9, is based on Beer's equation, which correlates over 1000 experimental results. Except for the work of one investigator, all the data agree with Beer's predictions of bubble radius to within 10%.

Parameter: $\dfrac{\mu_L \rho_V^{3/5} N_{holes}^{3/5}}{\Delta\rho g^{1/5} \dot{m}_V^{3/5}} + \left(\dfrac{\rho_L}{\Delta\rho}\right)^{0.1}$

Dimensionless volume $V g^{3/5} \dfrac{\rho_V^{6/5} N_{holes}^{6/5}}{\dot{m}_V^{6/5}} + \left(\dfrac{\rho_V}{\Delta\rho}\right)^{1/5}$ of fluid particles

Not valid for $1.01 > \dfrac{\rho_V}{\rho_L} > 0.99$

500
200
100
50
20
10
5
2
1.5
1.3
1.1
1.01
1.0

Dimensionless hole diameter $\dfrac{D_{or} \, \sigma \, \rho_V N_{holes}}{\Delta\rho g^{2/5} \dot{m}_V}$

$D/D_{We=1}$ for fluid particles

D^2 or $\Delta\rho g/\sigma = .1$
0.5
0.3
0.1
0.03
0.01

Weber number $= \dfrac{V_{or}^2 \, D_{or} \, \rho_V}{\sigma_{VL}}$
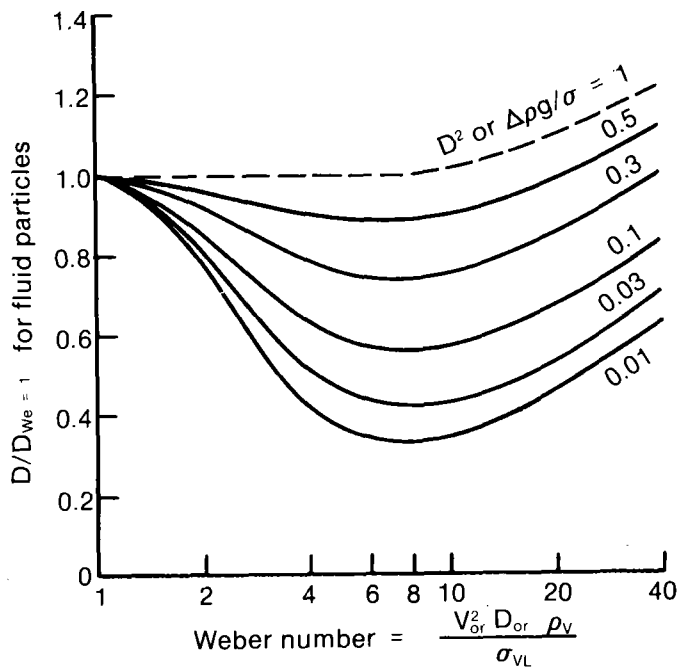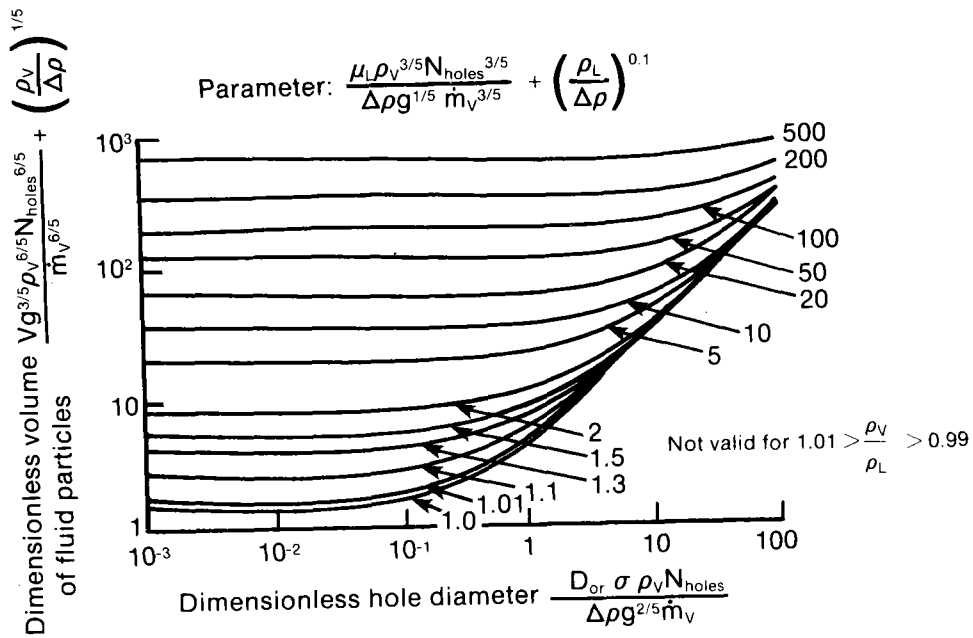
Figure 4-9. Bubble Production from Orifices

22

The pressure drop across the orifice when a bubble is formed is calculated using the nomograph reproduced in Figure 4-10. Smith and Van Winkle (1958) measured the pressure drop experienced by air flowing through an orifice plate and put their results in the form

$$\Delta P = K \left(\frac{\dot{m}}{CA_f Y}\right)^2 \frac{1 - (A_f/A_t)^2}{2 \, g\rho} \, ,$$

where $\dot{m}$ is the mass flow rate of the fluid (kg/s); A_f and A_t are the collective area of the holes and the total plate area (m^2), respectively; Y is the expansion factor and is approximately 1 for the system under consideration; g is the acceleration due to gravity (m/s^2); ρ is the density of the fluid upstream of the orifice plate (kg/m^3); and ΔP is the pressure drop across the orifice (Pa). C is obtained from Figure 4-10, and K is a conversion factor, equal to 9.8, that puts the results in the metric units given above. Smith and Van Winkle's results show the dependence of C on Reynolds number, hole diameter and spacing, and plate thickness.

4.3 PACKED-BED CONDENSER

The third type of condenser, shown in Figure 4-11, consists of a column filled with packing. Brine enters the column from the top and forms a thin film on the packing. Pentane vapor enters from the bottom and condenses on the brine, and the brine and pentane liquid leave together through a hole in the bottom of the column.

The packed-bed condenser is sized as follows: heat transfer relationships are given in terms of a volumetric heat transfer coefficient, which determines the
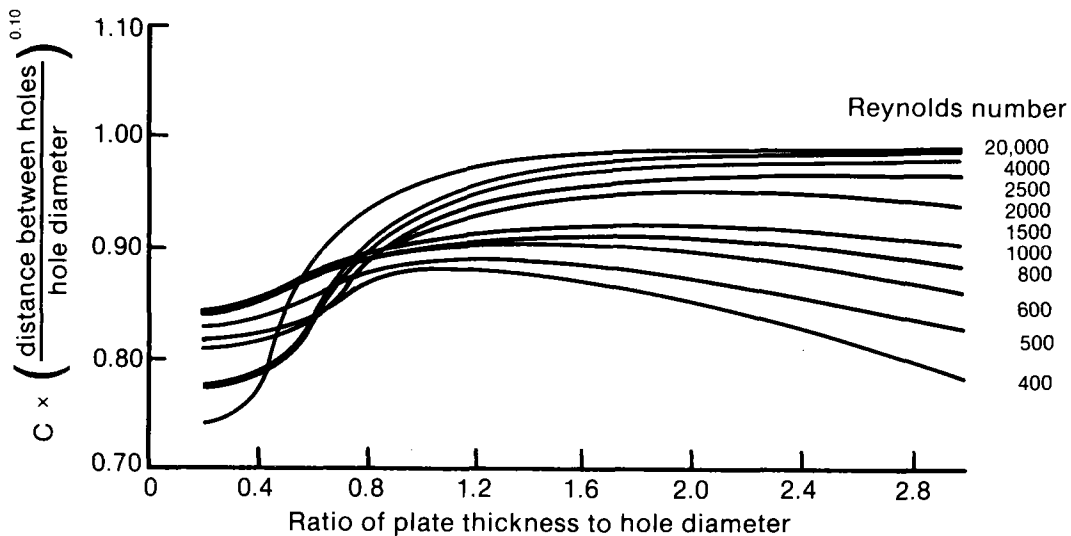
Source: Smith and Van Winkle 1958

Figure 4-10. Orifice Plate Coefficient C

SERI ⬤ ───────────────────────────
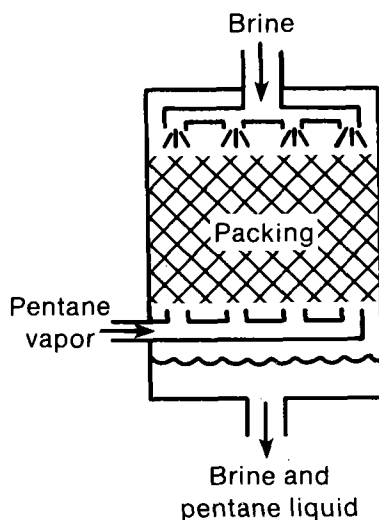
Figure 4-11. Schematic Drawing of a Packed-Bed Condenser

active volume of the condenser. The cross-sectional area is chosen to give a desired vapor-side pressure drop for the flow rates and type of packing under consideration. The heat transfer correlation used in this analysis is described in Section 4.3.1, and the superficial-velocity/pressure-drop relationship, which gives the cross-sectional area, is presented in Section 4.3.2.

One advantage of this condenser design is that condensation occurs with the two fluids in counter-flow. Another advantage is the low vapor-side pressure drop. The dis-advantages are the necessity of separating the brine and pentane, and the fairly high parasitic losses. Parasitic losses occur because the height that the brine falls over the packing is non-recoverable.

4.3.1 Heat Transfer in Packed-Bed Condenser

An experimental heat transfer correlation formulated by Jacobs, Thomas, and Boehm (1979) is used in this analysis. Jacobs, Thomas, and Boehm studied the condensation of R-113 on fresh water in a packed bed and compared their results to those of previous investigators' experiments on the condensation of steam on Aroclor and of methylene chloride on water. They correlated the data in terms of the following important dimensionless quantities: the Jakob number $Ja = h_{fg}/[C_{pv} (T_{sat} - T_{avg})]$, a modified Stanton number $St* = U_v A/[\dot{m}_v C_{pv} a (a_w/a_t)]$, a dimensionless column height $Z' = Z/D_p$, and a ratio of the products of mass flow rates and specific heats for the vapor and coolant, $B = \dot{m}_L C_{pL}/(\dot{m}_v C_{pv})$. [In these expressions, h_{fg} is the heat of vaporization (J/kg); C_{pv}, the specific heat (J/kg °C); T_{sat}, the saturation temperature (°C); and $\dot{m}_v$, the mass flow rate (kg/s), of the vapor. T_{avg} is the average temperature (°C); C_{pL}, the specific heat (J/kg °C); and $\dot{m}_L$, the mass flow rate (kg/s) of the coolant; a, the specific area (m²/m³); a_w/a_t, the ratio of wetted to total area (dimensionless); and D_p, the characteristic diameter (m) of the packing. A is the cross-sectional area (m²); Z, the height (m); and U_v, the volumetric heat transfer coefficient (W/m³ °C) of the condenser.] Somewhat surprisingly, they found no dependence on the thermal conductivity of the condensate although the experiments involved fluids with a large range of thermal conductivities. They obtained the correlation

$$St* = 0.40 \ B^{-0.21} \ H^{-0.67} \ Ja \ .$$

Jacobs now considers a theoretical approach to packed-bed heat transfer more reliable then the experimental correlation given here. Jacobs, Bogart, and

Pensel (1982) theoretically predict the condensation rate on an adiabatic sphere wetted by coolant. They adapt their results to conventional tower packings by treating each piece of packing as a sphere of the appropriate wetted area and assuming that coolant and condensate come to the same temperature as they fall from one piece of packing to the next. According to Jacobs, this approach predicts a more rapid condensation rate than the one reported by Jacobs, Thomas, and Boehm, probably indicating the presence of some noncondensables in the experiment.

4.3.2 Vapor-Side Pressure Drop in Packed Columns

Tower packings are designed to provide a high wetted surface area and low vapor-side pressure drop. Packing manufacturers provide plots such as Figure 4-12, which relate flow rates, areas, densities, viscosities, and pressure drops. The plot shows that for a given ratio of brine and pentane flow rates, pressure drop increases as area decreases (i.e., as the free area through which the vapor must pass gets smaller).

Different types of packing are represented by different packing factors F, given in the figure for packings considered in this report. In general, larger packings give lower pressure drops for given flow rates and cross-sectional areas.

4.4 DEAERATOR AND DEGASSER

The deaerator and the degasser have essentially the same design, since their function is the same: to remove a small quantity of dissolved material from the brine stream. A schematic of the deaerator is shown in Figure 4-13. The deaerator is a packed column maintained at low pressure. Brine enters the top of the deaerator and falls onto the packing, where it forms a thin film. This facilitates gas desorption, since it exposes a very large surface area. The desorbed gas is vented to atmosphere by compressors. The degasser works exactly the same way, but the desorbed gas, mainly pentane, is returned to the condenser by compressors. Gas desorption requirements determine the number of transfer units (described below) in the column, a function of both the area and height of the column.

The desorption requirements are so stringent that the deaerator and degasser both experience large parasitic losses, both from brine head loss and from the work of the compressors. As in the packed-bed condenser, the height that the brine falls over the packing is nonrecoverable. The work of the compressor is computed assuming adiabatic compression.

The deaerator and degasser operate under the principle of Henry's law, which states that the equilibrium concentration of a sparsely soluble gas in a liquid is directly proportional to the partial pressure of the gas above the liquid. The constant of proportionality is called Henry's constant, H, and is

Figure 4-12.   Gas-Liquid Packed Tower Correlations
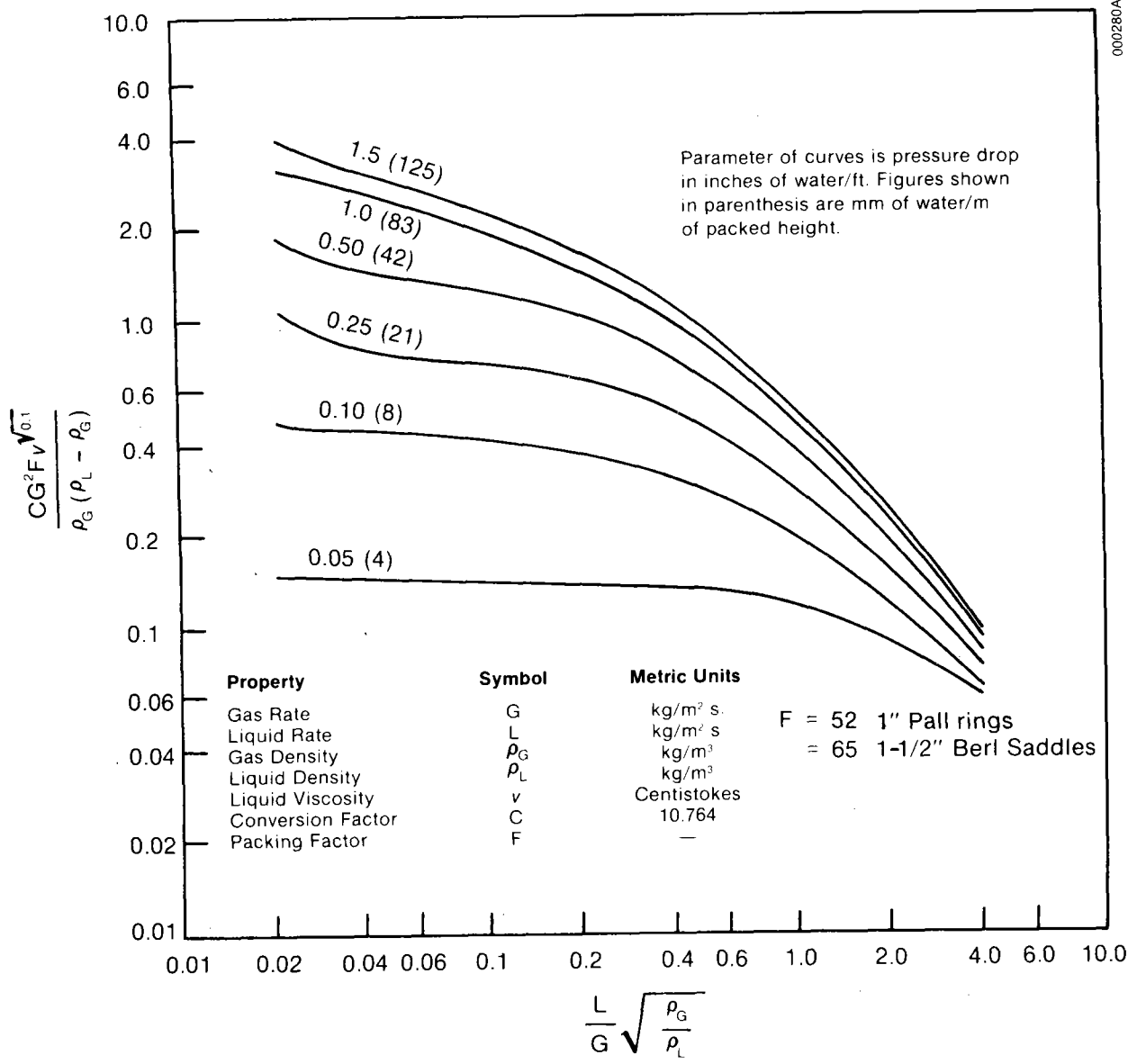
(Source: Norton Chemical Process Products Bulletin, reproduced
          from Wright 1982, in his notation)
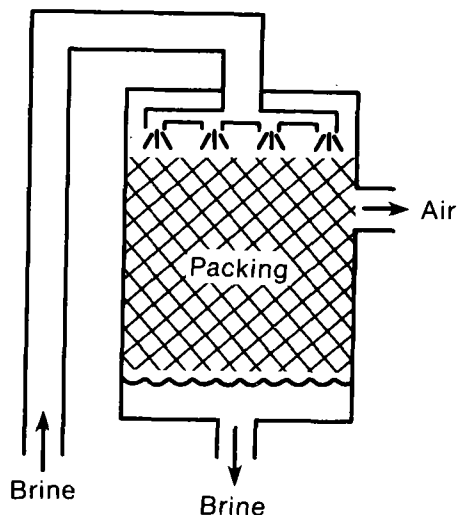
Figure 4-13. Schematic Drawing of a Deaerator

shown in Figure 2-4 for pentane dissolved in brine of various concentrations. Henry's constant for air in 25% salt water is approximately 4.18 ppm/atm.

The deaerator is maintained at a very low pressure, P_{da}, and the partial pressure of the air over the brine in the deaerator is $P_{da} - P_{brine}$, where P_{brine} is the saturation pressure of brine at that temperature. Thus, the equilibrium concentration of air in the brine in the deaerator is $X_{a_{eq}} = H(P_{da} - P_{brine})$, and can be reduced as much as desired by reducing the deaerator pressure. However, the brine will not reach this equilibrium concentration in the deaerator. How close it comes depends on residence time, initial concentration, flow rate, and surface area exposed.

We used the correlation of Golshani and Chen (1981) to predict the rate of approach to equilibrium. Their correlation is based on experiments on the desorption of air from fresh water, and was intended for use in the open-cycle ocean thermal energy conversion program. It is expressed in the form recommended by Sherwood and Holloway for mass transfer in a packed column.

$$ HTU = \frac{1}{\alpha} \left[\frac{\dot{m}_L}{A} \frac{1}{\mu_L} \right]^n \left[\frac{\mu_L}{\rho_L d} \right]^{0.5} , $$

where α and n are experimentally determined numbers that depend on the size and type of packing; μ_L is the viscosity (kg/ms); ρ_L, the density (kg/m^3); and $\dot{m}_L$, the mass flow rate (kg/h) of the liquid; d is the diffusivity of the gas in the liquid (m^2/h); and A is the cross-sectional area of the column (m^2). Values for α and n are given in Table 4-1. Since this equation is dimensional, the correlation should be used only in the units given above, which are, in some cases, different from the units given in the nomenclature of this report.

The correlation is expressed in terms of a height of transfer unit (HTU), related to the desorption rate as follows: the concentration, X, of a gas in the brine decays exponentially, approaching its equilibrium value, as shown in Figure 4-14. The desorption rate can be expressed by the equation

$$ e^{-NTU} = \frac{X_{out} - X_{eq}}{X_{in} - X_{eq}} , $$

Table 4-1. Coefficients in the Correlation of Golshani and Chen

Packing	α	n
3.81-cm ceramic Raschig ring	19.57	0.25
2.54-cm plastic Pall ring	113.6	0.34
3.81-cm plastic Pall ring	34.86	0.28

where X_{in}, X_{out}, and X_{eq} are, respectively, the initial, final, and equilibrium concentrations of gas in the brine in the column. This equation serves as the definition of the number of transfer units (NTU). The HTU is the height of column required for one NTU. If HTU is small, then gas is desorbed quickly. Figure 4-15 shows HTU plotted against cross-sectional area for the desorption of air and pentane from brine for the flow rate of interest. Golshani and Chen give an upper limit on flow rate per unit area for each of the packings they consider, listed in Table 4-1 and represented by the point at which the curve of Figure 4-15 begins. This limit is the "loading point" calculated by the method of Treybal. As area is decreased beyond this point, gas-side pressure drop increases rapidly, and desorption is hindered. In the range above this limit, the area can be chosen through a rough trade-off between deaerator cost and parasitic losses.
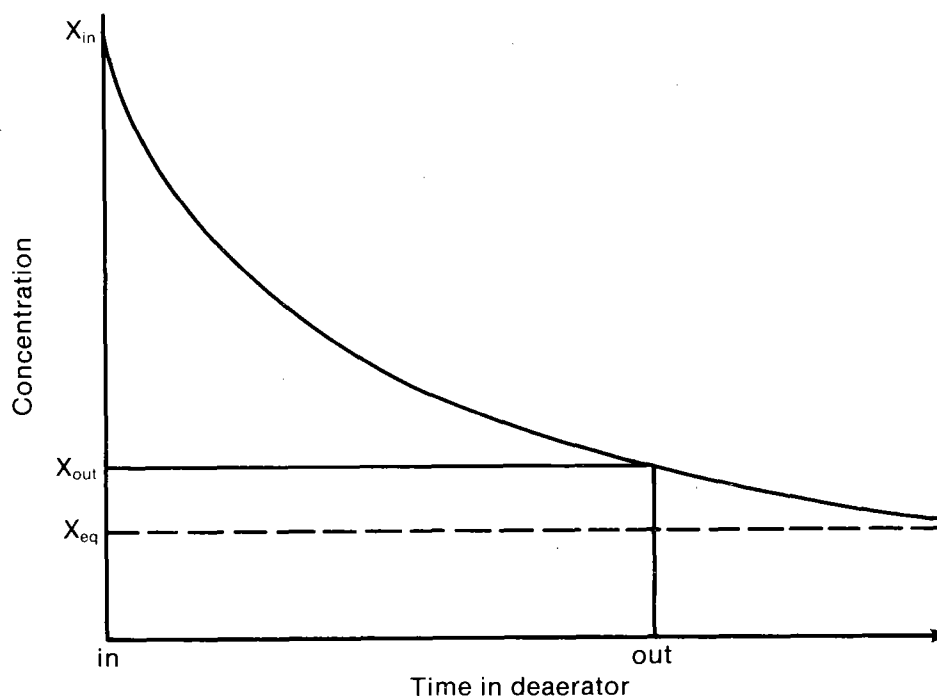
Figure 4-14. Concentration of Dissolved Air in Deaerator Brine
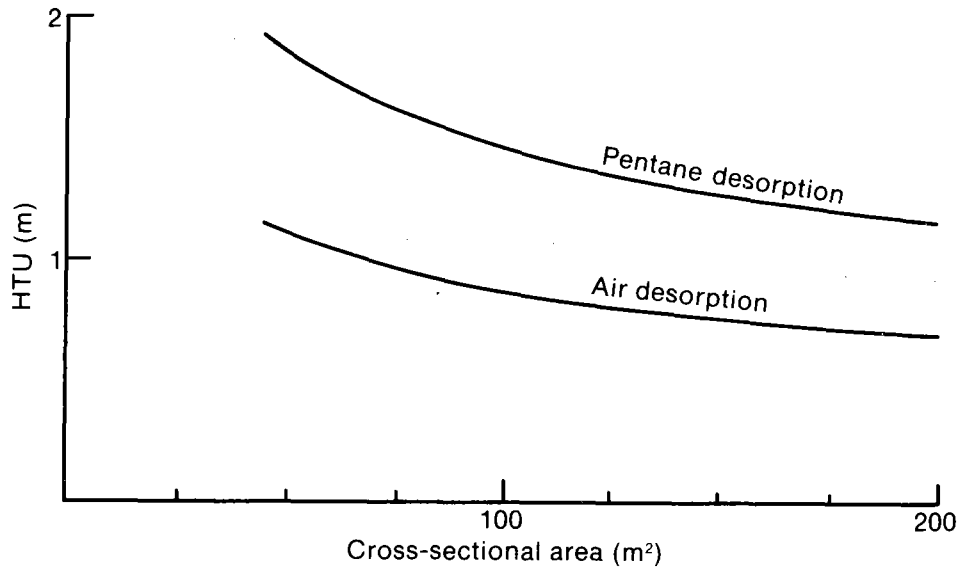
Figure 4-15. HTU of Deaerator and Degasser

SECTION 5.0

RELATIONSHIPS USED IN SIZING SHELL-AND-TUBE CONDENSER SUBSYSTEMS

In this section, we summarize the well-known and widely used relationships for sizing and calculating parasitic losses of shell-and-tube condensers and cooling towers. These relationships, cited in various handbooks, elementary texts, and costing articles, were used to size the shell-and-tube subsystem.

5.1 SHELL-AND-TUBE CONDENSER

The shell-and-tube condenser consists of a group of tubes inside a pressure vessel. The coolant (water) flows through the tubes, and pentane vapor, which fills the rest of the vessel, condenses on the outside of the tubes. We neglect any vapor-side pressure drop in the condenser under the assumption that it is very small in a well-designed condenser. The main source of parasitic losses for this type of condenser is the brine head loss due to friction with the tube wall. The sizing of the shell-and-tube condenser is done on the basis of a rough design, taking into account only the diameter and total surface area of the tubes. All effects of the configuration of tubes are neglected. The surface area required for heat transfer is calculated from the overall heat transfer coefficient. The correlations used for this coefficient are given in Section 5.1.1. Parasitic losses are calculated from frictional head loss correlations described in Section 5.2.1.

5.1.1 Heat Transfer in Shell-and-Tube Condenser

Heat transfer relationships for a shell-and-tube heat exchanger are usually experessed in terms of an overall heat transfer coefficient, U_s (W/m^2 $^\circ$C). U_s relates the heating or cooling load, Q (W), to the outside surface area of the heat exchanger, A_o (m^2), and the log mean temperature driving force ΔT_{LM}, ($^\circ$C), as follows: $Q = U_s A_o \Delta T_{LM}$. The overall heat tranfer coefficient is the reciprocal of the sum of all the resistances to heat transfer between the two fluids separated by the tube wall per unit area:

$$U_s = \cfrac{1}{1/h_o + r_{fo} + \cfrac{D_o \ln (D_o/D_i)}{2 k} + \cfrac{A_o}{A_i} r_{fi} + \cfrac{A_o}{A_i} \cfrac{1}{h_i}} ,$$

where h_o and h_i are the film heat transfer coefficients outside and inside the tube (W/m^2 $^\circ$C); r_{fo} and r_{fi} are the thermal resistances due to fouling on the outside and inside of the tube (m^2 $^\circ$C/W); D_o and D_i are the outer and inner diameters of the tube (m); k is the thermal conductivity of the tube material (W/m $^\circ$C); and A_o and A_i are the outside and inside surface areas of the tube (m^2). The resistances are arranged in the order that they occur, from the outside to the inside. The A_o/A_i factors are necessary in the latter terms because U_s is defined in terms of the outside area of the tube. The film heat transfer coefficients for deposits (the reciprocals of the fouling resistances r_{fo} and r_{fi}) are tabulated for common heat exchange fluids by Perry and Chilton (1973). From the values given for heated boiler feed water and

organic condensing vapors, the same resistance due to fouling is obtained for the outside and the inside, 1.761×10^{-4} m^2 °C/W. The resistance of the tube wall is easily obtained from the thermal conductivity of the material and from tube size. The correlations for film heat transfer coefficients h_o and h_i are described below.

The coefficient for heat transfer from the brine inside the tubes to the tube wall, h_i, is given by the empirical Sieder-Tate equation for fully turbulent flow (Perry and Chilton 1973). The equation relates the Nusselt number Nu = $h_i D_i / k_L$ (where k_L is the thermal conductivity of the liquid), the Reynolds number Re = $D_i V_L \rho_L / \mu_L$ (where V_L is the velocity, ρ_L the density, and μ_L the viscosity of the liquid), and the Prandtl number Pr = $C_{pL} \mu_L / k_L$ (where C_{PL} is the specific heat of the liquid).

$$Nu = 0.023 \ Re^{0.8} \ Pr^{1/3} \left(\frac{\mu_{L \ bulk}}{\mu_{L \ wall}} \right)^{0.21}$$

We set the final term equal to one, on the assumption that the liquid bulk and wall viscosities are approximately equal.

The film coefficient for condensation h_o on the outside of a single horizontal tube is given by a theoretical equation derived by Nusselt:

$$Nu = 0.73 \left(\frac{D_o^3 \ \rho_c^2 \ g \ h_{fg}}{\mu_c k_c \Delta T} \right)^{1/4} \ ,$$

where the Nusselt number and D_o are defined as before; ρ_c is the density (kg/m^3); h_{fg}, the heat of vaporization (J/kg); k_c, the thermal conductivity (W/m °C); μ_c, viscosity (kg/ms) of the condensate; ΔT is the temperature difference (°C) between the saturated vapor and the tube surface; and g is the acceleration due to gravity (m/s^2). For a collection of horizontal tubes, Nusselt's model requires a modification to the film coefficient predicted above. To account for the thickening of the condensate layer, the coefficient must be divided by $N^{1/4}$ where N is the number of tubes aligned vertically. However, experimental data have shown that Nusselt's model underpredicts the film coefficient for a single tube considerably, and the assumption of laminar flow makes the correction for bunches of tubes conservative as well. For those reasons, following the Perry and Chilton (1973) recommendation that the correction factor be omitted for inviscid condensates, we used the relation above to size the condensers for this study.

5.1.2 Parasitic Losses in Shell-and-Tube Condenser

Parasitic losses due to frictional head loss inside the tubes depend on tube diameter, length, and roughness, and on coolant velocity. Tube diameter and coolant velocity are specified in Section 7.2, following recommendations for geothermal power plants. The material of the heat exchanger is selected in that section as well. Using this information, heat transfer relationships described in the preceding section determine the total tube surface area, and thus the length of the tubes.

The Stanton-Moody diagram for friction in pipe flow can be used to calculate a friction factor from the quantities listed above and the physical properties of the liquid. The friction factor f is related to pressure drop by the following equation:

$$\Delta P = f \frac{L}{D_i} \frac{\rho_L V^2}{2} \, ,$$

where ΔP is the pressure drop (Pa), L and D_i are the length and inner diameter of the tube (m), and ρ_L and V are the density (kg/m³) and velocity (m/s) of the liquid. From the pressure drop, the parasitic loss, or the power required to pump the liquid through the tubes, is easily calculated, as power loss $p = (\dot{m}_L/\rho_L) \Delta P$, where $\dot{m}_L$ is the liquid mass flow rate.

5.2 COOLING TOWER

The mechanical draft cooling tower is a direct-contact counter-flow heat exchanger, in which the cooling water transfers heat to the air by evaporation as well as forced convection. Since cost correlations are available for cooling towers as a function of flow rates and temperatures, it is not necessary to size the cooling tower in any detail.

There are two main sources of parasitic losses in the cooling tower. The water loses head nonrecoverably as it falls down the tower, and work is required to blow air through the tower. The first contribution to the parasitic losses can be computed from the flow rate and tower height. Perry and Chilton (1973) provide estimates of tower height, but only for systems in which the liquid must be cooled by approximately 15°C, considerably more than our plant requires. Assuming that tower height is roughly proportional to cooling load for a given flow rate, I calculated the height requirement to be approximately 3.5 m. The contribution of the fans to parasitic losses is computed using an empirical formula provided by Vatavuk and Neveril (1981). $p = C_{adjusted} \times 0.497$, where p is the power of the fans (W) and $C_{adjusted}$ is the adjusted cost of the cooling tower ($) from their costing nomograph.

SECTION 6.0

SIZE AND COST OF DIRECT-CONTACT CONDENSER SUBSYSTEMS

In this section, we size and cost the three direct-contact condenser subsystems, using the correlations presented in Section 4.0 and following the procedure described in Section 3.0. In Section 6.1, the components of each of the condenser subsystems are sized for a pentane flow rate of 115 kg/s. In Section 6.2, parasitics are listed and thermal efficiency is computed for each of the three plant designs. Then, in Section 6.3, each of the condenser subsystems is scaled up for a plant producing 5 MW_e net, and costed. All types of plants are scaled up to 5 MW_e for comparison in Section 8.0.

6.1 INITIAL SIZING

This section describes the design of the three direct-contact condensers, the settling tanks, and the deaerator and degasser. These components are sized so that their parasitic losses can be evaluated. The three condensers are sized in Sections 6.1.1 through 6.1.3, and the deaerator and degasser in Section 6.1.4. The settling tank is not sized until Section 6.2, since its parasitics are negligible.

6.1.1 Drop-Type Condenser

The main design variable for the drop-type condenser is the drop size, which determines residence time and terminal velocity. Drop size depends on spray nozzle size and pressure drop, as shown in Figure 6-1, provided by Spraying Systems Co. The different curves describe the performance of different spray nozzles. Information about the capacities of these nozzles at various flow rates is provided by the manufacturer on a separate sheet. Drop size increases with nozzle size for a given pressure drop, and decreases with pressure drop for a given nozzle.

The pressure drops for which drop size information is provided are considerable. The smallest pressure drop shown is 68.95 kPa (10 psi), which corresponds to a parasitic loss of 155 kW (3% of the plant output) for the brine flow rate under consideration. For that reason, we considered only nozzles operating at the lowest pressure drop. At this pressure drop, we had to choose among nozzles of different capacities. This choice involved a rough trade-off between condenser height (and thus gravitational parasitic losses) and condenser area (which depends on the number of nozzles). Small nozzles produce small drops which require small heights for condensation. However, a large number of small nozzles, and thus a large cross-sectional area, is required. We calculated dimensions of the drop-type condenser for several sizes of spray nozzles operating with that pressure drop and selected a nozzle which has a capacity of approximately 0.89 kg/s. The median drop diameter, shown on the figure, is 650 microns.

The condenser was designed for a drop with twice the median diameter, for the reasons mentioned in Section 4.1. Heat transfer relationships (see

33

(The curves represent different nozzle sizes.)

Particle size: median volume diameter (μm)

psi

kPa

Pressure drop across nozzle
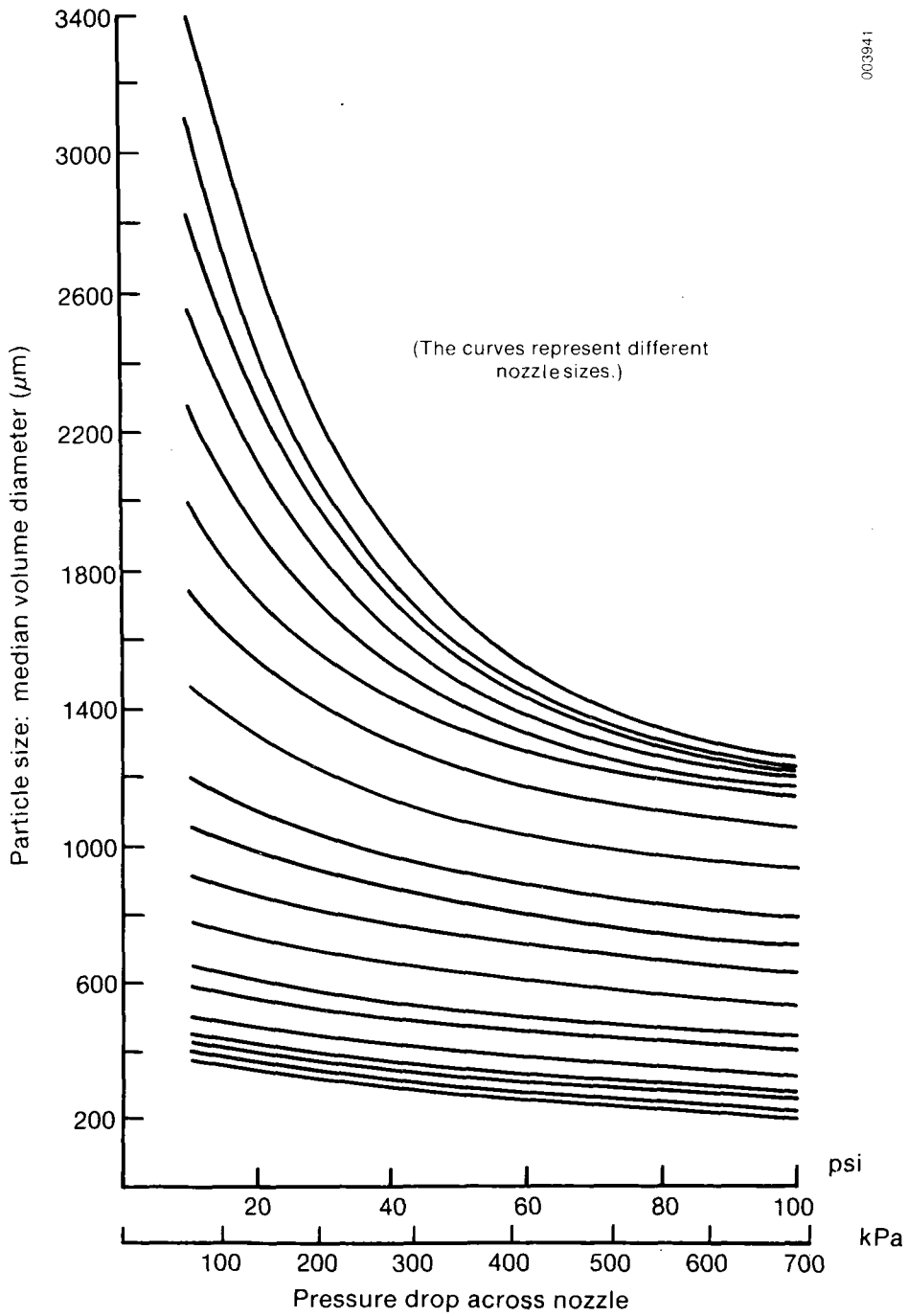
Source: Spraying Systems Co.

Figure 6-1. Drop Size (The different curves represent different nozzle sizes)

Source: Spraying Systems Co.

Figure 4-3) gave a residence time requirement of 0.43 seconds for a 1.3-mm-diameter drop under the operating conditions of the condenser. This corresponds to an active height of 1.98 m (see Figure 4-4). The condenser itself must be somewhat taller than this (3.0 m) to allow space for the spray nozzles and brine distribution system, but only the active height contributes to parasitic losses.

The cross-sectional area of the condenser is chosen on the basis of nozzle spacing. We arbitrarily chose to place the nozzles 25 cm apart, in an equilateral triangle arrangement. Thus, since approximately 3000 spray nozzles are required, the condenser must have a cross-sectional area of 163 m^2. Since cost information is not readily available for pressure vessels of this size, we chose to design this condenser (and other large system components) as a group of smaller units in parallel. Each unit has a diameter of 3.65 m (12 ft) or less, so that it can be transported by truck from the manufacturer to the plant site. The drop-type condenser will consist of 16 units of this sort.

6.1.2 Bubble-Type Condenser

Condenser dimensions are determined by the size of the particles of the dispersed phase for this design, as they were for the drop-type condenser. However, this parameter can not be varied freely. Bubbles must initially be between 4 and 8 mm in diameter to guarantee an essentially constant rise velocity. We selected an intermediate value for the design, 6 mm. This sort of drop can be produced through orifices that are 1 mm in diameter. The number of holes is chosen to prevent weeping. If vapor flow rate through an orifice is low, then brine from above the plate may "weep" down into the chamber containing the vapor. Mersmann (1978) supplies a correlation that gives a minimum flow rate through each hole or, equivalently, a maximum number of holes for a given total flow rate, to prevent this phenomenon. We use the maximum number of holes, 7,834,000, to keep the vapor-side pressure drop low. Once the number and size of holes have been selected, the pressure drop across the orifice can be computed, using the correlation of Smith and Van Winkle. The pressure drop of the vapor as it passes through the orifice is calculated to be approximately 100 Pa.

Once the bubble size is known, cross-sectional area can be estimated on the basis of bubble spacing. If 7,834,000 holes must be placed one diameter (or 6 mm) apart, on the vertices of equilateral triangles, then a cross-sectional area of 245 m^2 is required. Like the drop-type condenser, this condenser will be built of smaller modules in parallel. Twenty-four modules are needed.

Bubble size determines the height required for heat transfer as well. The heat transfer relationship of Jacobs, Beggs, and Fannar, along with terminal velocity correlations, predicts a very small active height for the condenser (only a few centimeters). However, the condenser must be designed with a much taller column of brine to avoid substantial entrainment of pentane.

We designed the condenser so that the lateral velocity of the brine at its outlets would be roughly the same as the rise velocity of the pentane bubbles. For a volumetric flow rate of 0.078 m^3/s per module, this leads to the requirement that the pentane exit pipe be at least 70 cm in diameter. In

order to reduce the size of the pipe, we chose to have two brine outlets (and two brine inlets), each with a diameter of 50 cm. This should promote a better flow arrangement in the condenser as well as reducing the height requirement. This choice of lateral velocity implies that bubbles should not be formed within a distance of 50 cm of the brine exit orifices, reducing the useful area of the condenser by 7% and necessitating two additional modules.

The actual height of each module will be 1 m, with a generous allowance for the height of the vapor chamber and the layer of pentane liquid above the brine. Since this is fairly short, several modules can be stacked to form larger pressure vessels. Figure 6-1 shows a pressure vessel that consists of 6 modules. It is less expensive than six individual vessels because the cost of ends and supports is greater than the cost of plates to separate a column into compartments.

Figure 4-5 shows the brine entering one side of a compartment and leaving at the other side. To prevent the formation of stagnant areas in the condenser, it is necessary to distribute the brine with a system of baffles. These baffles have not been designed, so their parasitic losses are not included in our calculations. The only parasitic loss included in the analysis of this condenser design is the small amount of extra work that must be done to pump the liquid pentane to boiler pressure. For each condenser design, work is required to pump the pentane from the turbine exit pressure (73.76 kPa) to the boiler pressure (300 kPa). In the bubble-type condenser, the pentane liquid starts at slightly lower pressure (67.81 kPa), equal to the turbine exit pressure minus the orifice pressure drop and the hydrostatic pressure of the layer of brine. The extra pumping work associated with this design is 1.3 kW, or less than 0.5% of the plant's output.

6.1.3 Packed-Bed Condenser

The correlation of Thomas, Jacobs, and Boehm expresses heat transfer in terms of a volumetric heat transfer coefficient, but the correlation determines the height, not the volume of the packed-bed condenser when it is put in dimensional form. Thomas, Jacobs, and Boehm performed experiments on two types of packing: 3.81-cm (1.5 in.) Berl saddles, and 5.08-cm (2-in.) Raschig rings. Our design uses Berl saddles, which require less height for heat transfer and a smaller cross-sectional area for a given vapor-side pressure drop. The column is designed for a pressure drop of 1.2 kPa per meter of height (1-1/2 inches of water per foot of height), with a 10% safety factor in area. According to the heat transfer correlation, the condenser must have an active height of 2.95 m. According to the flow rate/pressure correlations reproduced in Figure 4-12, the condenser must have an area of 91 m^2. This corresponds to 9 modules. The main source of parasitics is the head loss of the brine as it falls over the packing. The power lost in this process is 77.4 kW.

6.1.4 Deaerator and Degasser

For a given deaeration load, the active height and area of the deaerator are interrelated. The duty of the deaerator can be described as a number of

transfer units (5.7 in this case) required to reduce noncondensables in the condenser to 1% by volume. The active height of the deaerator is the product of a number of transfer units (NTU) and height of a transfer unit (HTU). Figure 4-15 shows how HTU decreases as area increases. So, the sizing of the deaerator involves a trade-off between the cost of increasing area and the cost (in enlarging the plant) of the parasitics caused by a large active height.

We made a rough calculation of the impact of parasitics on plant cost for comparison with the cost of enlarging the deaerator and concluded that the least expensive design was the one with the smallest deaerator cross-sectional area permitted by flooding considerations. The same conclusion applies to degasser design.

Both the degasser and the deaerator use 2.54-cm (1-in.) plastic Pall rings as packing. According to the flooding calculations of Golshani and Chen, the maximum flow rate per unit area is 47.5 kg/s m^2, which corresponds to a cross-sectional area of 56.3 m^2 for the system under consideration. We applied a safety factor of 10% and arrived at a cross-sectional area of 62 m^2.

The deaerator and degasser operate at low pressures (between 2 and 3 kPa, where about 2 kPa corresponds to the partial pressure of the brine). Because they are at lower pressures than either the preceding or following points in the brine loop, brine must be pumped out of them. To reduce the work of pumping somewhat, the brine enters the degasser and deaerator by barometric lift. Some of the brine's energy, lost when pressure is reduced, is converted into recoverable gravitational potential energy.

For the design conditions, Figure 4-15 shows that the HTUs for air and pentane desorption are, respectively, 1.14 m and 1.90 m. The NTUs set by the desorption requirements are 5.7 for air and 4.4 for pentane. This leads to a deaerator with an active height of 6.5 m, and a degasser with an active height of 8.4 m. These heights correspond to parasitic losses of 170.6 kW and 219.7 kW, respectively. The other source of parasitic losses is the work of the compressors that remove the desorbed gases and whatever water vapor is released. In the deaerator, the compressor work is 34.1 kW; in the degasser it is 9.2 kW. There are two reasons for the difference in the work of the compressors. Although the mass fractions of air and pentane released from the brine are comparable (on the order of 4 ppm), the volume of pentane vapor to be compressed is much smaller than the volume of air. The second reason for the difference is less important. The deaerator compressor returns air to atmospheric pressure while the degasser compressor returns pentane vapor to the condenser, overcoming a smaller pressure difference.

6.2 PLANT EFFICIENCY

The parasitic losses of the three direct-contact condenser subsystems and of the rest of the power plant are summarized in Table 6-1. Parasitic losses due to pipe friction are neglected since they should be more or less the same for all the plant designs. Section 7.2 describes how the parasitics of the rest of the plant were calculated, and lists the efficiencies assumed for pumps and compressors.

Table 6-1. Parasitic Losses

Direct-Contact Condenser Subsystems	
Deaerator	
Gravity headloss	213.2 kW
Compressor work	48.7 kW
Condensers	
Drop-type condenser	
Nozzle headloss	194.9 kW
Gravity headloss	65.0 kW
Bubble-type condenser	
Extra pumping for pentane liquid	1.3 kW
Packed-bed condenser	
Gravity headloss	96.8 kW
Degasser	
Gravity headloss	274.6 kW
Compressor work	13.1 kW
Total for drop-type condenser subsystem	809.5 kW
Total for bubble-type condenser subsystem	550.9 kW
Total for packed-bed condenser subsystem	646.4 kW
Rest of the Plant	
Work of pumping pentane from condenser to boiler	53.8 kW
Work of pumping brine from pond to boiler	256.4 kW
Total for the rest of the plant	310.2 kW

The efficiency of each plant is calculated from parasitics and thermodynamic information as follows. Efficiency is defined as the ratio of useful work leaving a system to heat entering the system. We know that the pentane absorbs 50.945 MW_t from the hot brine as it passes through the boiler, and that it rejects 44.9305 MW_t in the condenser. The difference between these two quantities (6.0145 MW_t) is converted to work in the turbine and then to electricity. This conversion process is assumed to have an efficiency of 90%, so the gross power output of the plant is 5.413 MW_e. The remaining 10% of the 6.0145 MW_t is heat generated either in the turbine or the power-generating equipment. We assumed that none of this remaining heat is reabsorbed by the pentane stream. The net useful work produced by the system (in the form of electricity) is found by subtracting the parasitic losses from the gross output of the plant. The parasitic losses from the condenser subsystem must be expressed in terms of the electricity required to operate pumps and compressors, i.e., the ideal work must be divided by the efficiency of the pump or compressor. Throughout this report, pumps are assumed to have an efficiency of 80%, and compressors, 70%. The parasitics listed in Table 6-1 are corrected for these efficiencies.

The parasitics of the rest of the plant are derived as follows. For an ideal pump, the power required to pump the pentane liquid from the condenser back to the boiler is the product of the pressure difference and the volumetric flow rate of the pentane. For a real pump, this power must be divided by the efficiency (0.8). Similarly, the power required to pump the brine from the solar pond to the boiler is $(\dot{m}_L/\rho_L) \, \Delta P/e_{pump}$. This is a considerable amount of work, more than 10% of the plant's electrical output. According to Wright's design, some of this work can be recovered if a hydraulic turbine is inserted between the boiler exit and the solar pond. If the hydraulic turbine has an efficiency of 70% and the mechanical work that it produces is used by the brine pump with an efficiency of 80%, then the power requirements can be reduced by slightly more than half.

Following the steps outlined above, we calculated the net useful output and efficiency for the plant for each design. These quantities are reported in Table 6-2.

6.3 SCALE-UP: SIZING AND COSTING

The designs of condenser subsystem components given in Section 6.1 are based on the same brine and pentane flow rates (2675.6 kg/s and 115 kg/s, respectively). Section 6.2 shows that the plants containing these subsystems produce different amounts of electricity. For a fair evaluation of the condenser subsystem choices, each plant must be enlarged to produce the same net amount of electricity (5 MW_e). For each plant, the pentane and brine flow rates must be multiplied by the ratio of desired output (5 MW_e) to output as designed in Section 6.1.

For the bubble-type condenser, for example, this ratio is 5/4.552. This scale-up procedure is used on the assumption that the same amount of electricity is produced per unit flow rate of pentane before and after scale-up, i.e., that cycle efficiency is unchanged by a small change in the size of the plant.

In this section, the three direct-contact condenser subsystems are scaled up and costed. The costing method is described in Section 6.3.1, and the three subsystems are enlarged and costed in Sections 6.3.2, 6.3.3, and 6.3.4. The cost of the rest of the plant scaled up to produce 5 MW_e is estimated in Section 8.0.

Table 6-2. Cycle Efficiency

Condenser	Useful Output (MW_e)	Efficiency
Drop-type	4.293	8.43%
Bubble-type	4.552	8.94%
Packed-bed	4.456	8.75%

6.3.1 Costing Method

We used the costing method of Pikulik and Diaz (1977) to estimate the cost of the system components. This is the method Wright used (1982) to estimate the cost of direct-contact boilers. The costs are given in 1977 dollars, which are converted to 1980 dollars using the Marshall and Swift equipment cost index provided by Chemical Engineering Magazine. All prices will be presented in 1980 dollars unless otherwise mentioned.

Diaz and Pikulik recommend the following costing procedure once the dimensions of a piece of equipment are known. First, the cost and weight of the material for the walls, ends, support, internals, and orifices are estimated using nomographs. Then, the cost of fabricating the equipment is calculated using the following empirical formula:

$$C_s = S \ (3.1D + 1.2L + 3M + N + W) \ ,$$

where C_s is the shop cost (or cost of fabricating); S is the hourly rate for shop labor, given by Pikulik and Diaz as $28.50 for the fabrication of towers; D and L are the diameter and height of the vessel; M is the number of manholes (2 in this analysis); N is the number of orifices; and W is the weight of material in tons. The material cost and shop cost are added to give the fabricated cost. Finally, the fabricated cost is multiplied by a factor between 1.25 and 1.16 to account for engineering and administrative costs, etc. The factor decreases as the fabricated cost increases. We assumed that it was a constant 1.16, the factor for items more expensive then $75,000, for the following reason. Although individual modules may cost less than $75,000, they would be part of an order of several identical items. Thus, the engineering and administrative costs should be applied at the rate given for large, expensive items.

The final result of this costing procedure is an F.O.B. cost, i.e., the total cost to be paid to the manufacturer before shipping. The costing of the deaerator for the drop-type condenser subsystem is described in detail, as an example, in Section 6.3.2.

6.3.2 Drop-Type Condenser Subsystem

Because of parasitic losses, the flow rates in the drop-type condenser subsystem must be increased by a factor of 5/4.293 to 134 kg/s for pentane and 3116 kg/s for brine. The increase in flow rates affects the cross-sectional area but not the height of the components. The cross-sectional area given in Section 6.1 must be increased by precisely the same factor as the flow rates.

The deaerator designed in Subsection 6.1.4 had an active height of 6.5 m and an area of 62 m^2. For cost estimates of the enlarged plant, the active height remains the same, but the total height of the vessel is 7.5 m to allow room for packing supports and a brine distribution system. The cross-sectional area is increased to 72 m^2. The deaerator will consist of 7 modules each 3.62 m in diameter. One such module is shown in Figure 6-2.
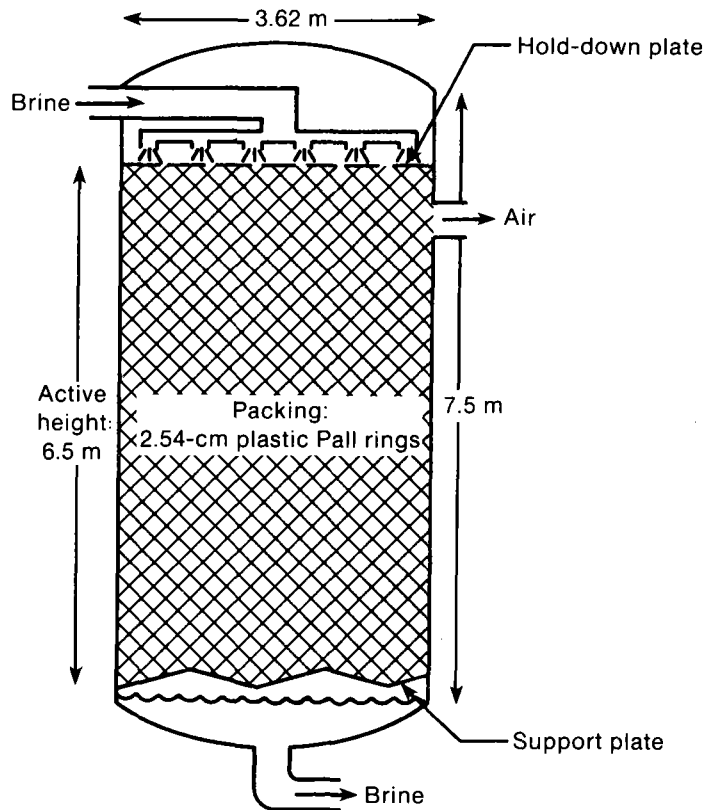
Figure 6-2. Deaerator Module. (Seven modules are required.)

Each module has 3 orifices (brine inlet and outlet and gas outlet), a packing support and bed limiter to hold the packing in place, two manholes, and a weir-and-trough distributor for the brine. The walls and ends of the vessel are made of 1.1-cm-thick (7/16-in.) carbon steel, and the vessel support is made of 0.6-cm-thick (1/4-in.) carbon steel. The active volume of the column is filled with 2.54-cm (1-in.) plastic Pall rings. The costs and weights of these items are listed in Table 6-3.

The total material cost of the deaerator is $63,300. The shop cost is $3200. This gives a fabricated cost of $66,500 and an FOB cost of 1.16 × $66,500, or $77,200. The 1980 cost is calculated by multiplying the 1977 cost by 659.6/505.4. It is $100,700. The cost for 7 units of this sort is $705,100.

The cost of the degasser is calculated in precisely the same way. The degasser is 9.4 m tall, of which 8.4 m is the active height. Since its total cross-sectional area is the same as that of the deaerator (72 m^2), the degasser too is built as seven modules in parallel. The cost of a single module is $118,300 the total degasser cost is $828,100.

SERI

Table 6-3. Cost of Deaerator for Drop-Type Condenser Subsystem

	Quantity	Unit Mass (kg)	Total Mass (kg)	Unit Cost ($)	Total Cost ($)
Walls	7.5 m	916/m	6,880	681/m	5,110
Skirt (i.e., support)	2.5 m	532/m	1,330	488/m	1,220
Caps	2	2,870	7,530	5,833	11,670
Packing	74.1 m^3	88.2/m^3	6,530	494/m^3	36,610
12 in. nozzles	2	68	140	630	1,260
3 in. nozzle	1	10	10	190	190
Manholes	2	300	600	1,500	3,000
Distributor	1	210	210	1,190	1,190
Support plate	1	3,600	3,600	1,090	1,090
Hold-down plate	1	8,940	8,940	1,990	1,990
Total material mass			33,960		
Total material cost					63,330
Shop cost					3,210
Fabricated cost					66,540
Engineering cost, etc.					10,650
F.O.B. cost (1977)					77,190
F.O.B. cost (1980 dollars)					100,700

The enlarged drop-type condenser is designed with a height of 3.0 m (active height 1.98 m), and a total area of 190 m^2. This area can be attained with 19 modules, each 3.57 meters in diameter. Each module costs $45,800. The total condenser cost is $870,000. One condenser module is shown in Figure 6-3.

Since brine and pentane liquid leave the condenser together for this design, a settling tank is required. We sized the tank to give the brine and pentane two minutes to separate. This requires a volume of 343 m^3 (90,600 gal). The Diaz and Pikulik method does not provide nomographs for such large vessels, so we used a correlation for large storage tanks provided by Guthrie (1969). For a 100,000-gal horizontal carbon-steel pressure storage vessel, Guthrie estimates a cost of approximately $64,300 (converted to 1980 cost). There is a great deal of uncertainty in this cost estimate because a settling tank may have quite a different cost from a storage tank of the same capacity, and because two minutes' residence time may not be adequate for full separation of the two liquids.

The pumps and compressors are the only remaining equipment in the condenser subsystem. The brine loses 265 kPa (38.4 psi) as it travels through the deaerator, condenser, and degasser. This means that pumps must perform on the brine at a rate of almost 700 kW. The height of the components of the condenser subsystem can be selected to allow this work to be added at any point in the loop. Pikulik and Diaz provide a nomograph for pump cost as a
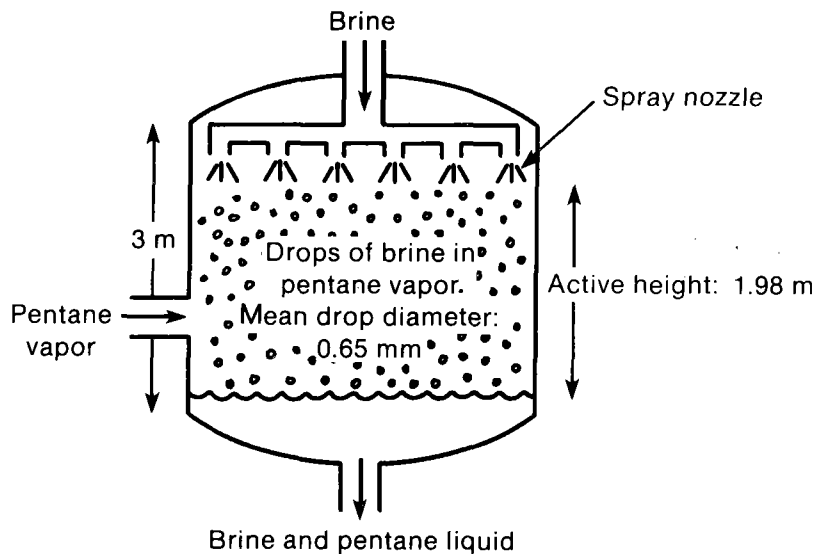
Figure 6-3. **Drop-Type Condenser Module** (Nineteen modules are required.)

function of the product of flow rate and pressure gain, but not for pumps large enough to carry the entire pumping load for this system. In order to use the correlation, we decided to use four pumps, each of which cost $23,500. The compressors for the deaerator and degasser, on the other hand, are smaller than those costed by Pikulik and Diaz. I extrapolated the curve and estimated that both would cost approximately $65,000.

The prices of the components of this condenser subsystem are summarized in Table 6-4 along with the costs of the condenser options. Since the costing procedure is very similar for the three options, only sizing information is presented in the text of the remainder of the section.

6.3.3 Bubble-Type Condenser Subsystem

The scaling factor for the bubble-type condenser subsystem is 5/4.552, which leads to a pentane flow rate of 126 kg/s and a brine flow rate of 2939 kg/s.

For these flow rates, the deaerator has a total area of 68 m^2, which can be achieved with 7 modules, each with a diameter of 3.52 m. The degasser area requirements are exactly the same, and the heights of both deaerator and degasser are unchanged from the drop-type subsystem design.

The condenser has a height of 1 m, of which 60 cm is filled with brine. Its area is 270 m^2, which corresponds to seven modules, each one consisting of a stack of 4 condenser units. The diameter of each module is 3.5 m.

SERI ☀

Table 6-4. Cost of Subsystems

	Number of Modules	Total Area (m^2)	Cost per Module ($)	Total Cost ($)
Drop-Type				
Deaerator	7	72	100,700	705,100
Condenser	19	190	45,800	870,000
Settler	1		64,300	64,300
Degasser	7	72	118,300	828,100
Pumps	4		23,500	94,000
Compressors	2			65,000
Total				2,626,500
Bubble-Type				
Deaerator	7	68	95,900	671,100
Condenser	7	270	72,600	508,400
Settler				
Degasser	7	68	112,600	787,900
Pumps	3		19,600	58,800
Compressors	2			65,000
Total				2,091,200
Packed-Bed				
Deaerator	7	70	97,800	684,600
Condenser	10		59,500	595,100
Settler	1	102	64,300	64,300
Degasser	7	70	114,800	803,900
Pumps	4		18,300	73,100
Compressors	2			65,000
Total				2,286,000

All costs in 1980 dollars.

This condenser subsystem does not require a settling tank. Costs of pumps and compressors and components described above are given in Table 6-4. Figure 6-4 is a drawing of the bubble-type condenser.

6.3.4 Packed-Bed Condenser Subsystem

The brine and pentane flow rates for this subsystem are, respectively, 3002 kg/s and 129 kg/s, corresponding to a scale-up factor of 5/4.456. The scale-up area requirement necessitates 7 deaerator modules and 7 degasser units, each with a diameter of 3.56 m. The heights of these components are unchanged from those given in Sections 6.1.4 and 6.3.2.
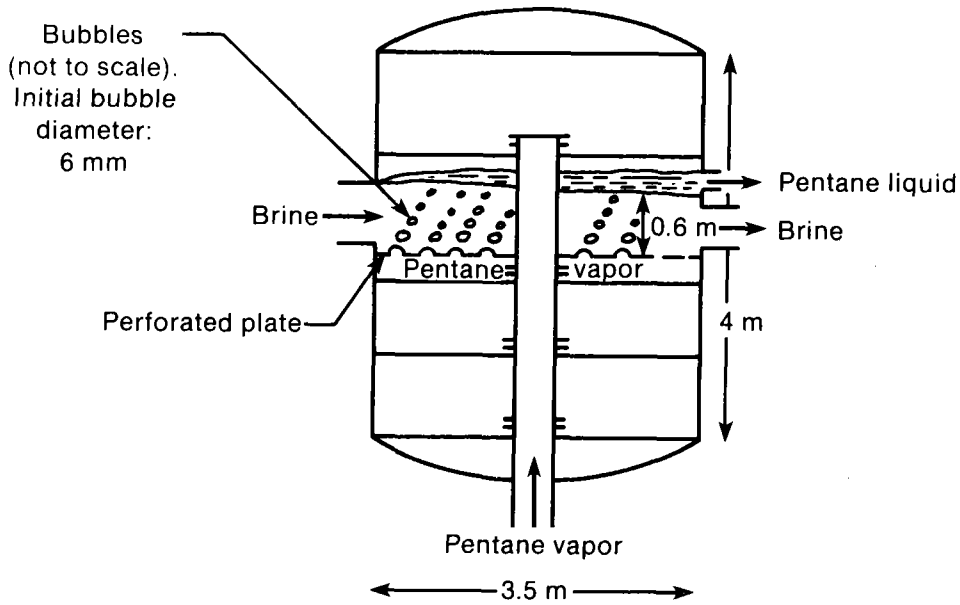
Figure 6-4. **Bubble-Type Condenser Module.** (Seven modules are required. Only one of the four compartments of this module is shown.)
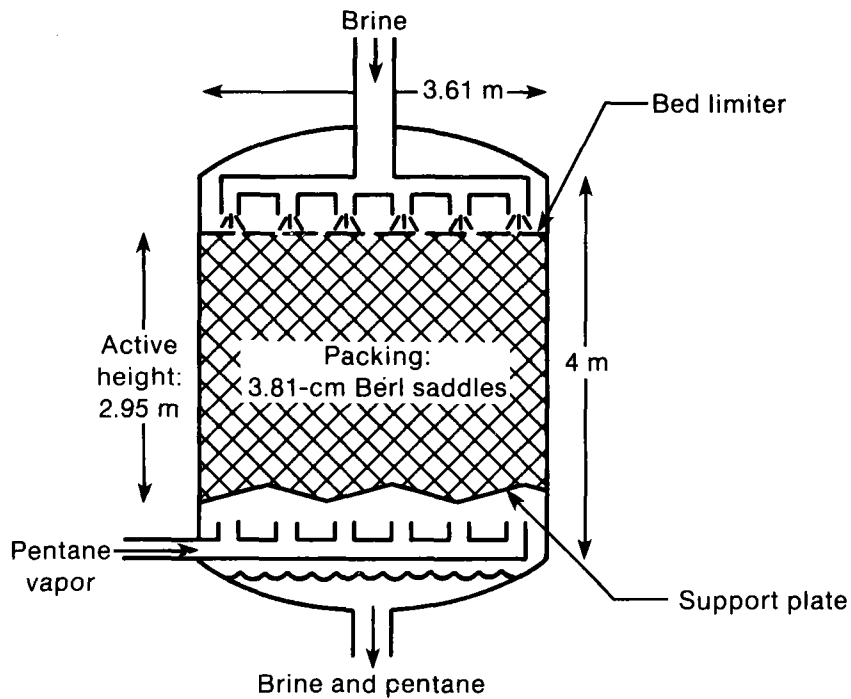
Figure 6-5. **Packed-Bed Condenser Module**

45

The condenser consists of 10 modules, each with a diameter of 3.61 m and an active height of 2.95 m. The physical height of each module is 4 m and the packing used is 3.81-cm (1.5-in.) Berl saddles. The costs of all the components of this condenser subsystem are given in Table 6-4, and a drawing of the packed-bed condenser is given in Figure 6-5.

SECTION 7.0

SIZE AND COST OF SHELL-AND-TUBE CONDENSER SUBSYSTEM

This section gives the sizing and costing of the shell-and-tube condenser subsystem, following the method outlined in Section 3.0 and using the correlations described in Section 5.0. In Section 7.1, we size the condenser subsystem to fit into the initial plant (with a pentane flow rate of 115 kg/s). In Section 7.2, we calculate the thermal efficiency of this plant. Section 7.3 contains a description of how the plant is scaled up to produce 5 MW_e net and how the size and cost of the condenser subsystem are computed for the larger plant. The cost of the entire enlarged plant is calculated in Section 8.0 and compared with the costs of the three direct-contact plants.

7.1 INITIAL SIZING

In order to use the heat transfer correlations presented in Section 5.1, it is necessary to select a tube diameter. Robertson (1980) recommends an outer diameter of between 1.6 and 2.5 cm for condensers in geothermal power plants. Below the lower limit, clogging of tubes is a problem. Above the upper limit, excessive amounts of coolant are required to attain 1.8 m/s, the coolant velocity desired for good heat transfer. We selected an intermediate value, 2.0 cm, as the tubes' external diameter, and 1.9 cm as the internal diameter. The tubes are assumed to be made of carbon steel, which has a thermal conductivity of 47.6 W/m ^{o}C.

Using this information, we calculated the film heat transfer coefficients. For condensation on the outside of the tube, the coefficient is h_o = 2700 W/m^2 ^{o}C. For heat transfer from the coolant inside the tube, the coefficient is h_i = 6030 W/m^2 ^{o}C. The overall heat transfer coefficient is U_s = 1090 W/m^2 ^{o}C, which is within the range given by Perry and Chilton for organic vapors condensing on tubes containing water. The surface area of the tubes required for the condensing load is calculated from the heat transfer coefficient and temperature change of the coolant to be 11,000 m^2.

The number of tubes required is N = $\dot{m}_L/(\rho_L VA_{tube})$ or 4144, where $\dot{m}_L$ is the mass flow rate of water (kg/s), V is the velocity of water in the tubes (m/s), ρ_L is the density of water (kg/m^3), and A_{tube} is the cross-sectional area of a tube (m^2). The length of the tubes is L = $A_s/(Na_s)$, or 42.2 m, where A_s is the surface area required (m^2) and a_s is the surface area per unit length of a single tube (m^2/m). From this information, we calculated the frictional head-loss of the water in the condenser, 189.8 kW.

We costed the cooling tower in order to compute the fans' contribution to parasitic losses. The costing plot of Vatavuk and Neveril (1981) is shown in Figure 7-1. First, a cost is read from the main plot. For a flow rate of 2.115 m^3/s and range (i.e., change in water temperature) of 5.6^{o}C (slightly more than is required), the cost is $180,000. Then, the cost is adjusted by two factors shown in the figure, which depend on the approach temperature (temperature difference between water leaving the cooling tower and air entering it) and the ambient wet-bulb temperature. These factors are not

(Range is the difference between water temperature at the inlet and the outlet of the cooling tower;
Approach is the difference between water exit and air wet-bulb inlet temperature.)
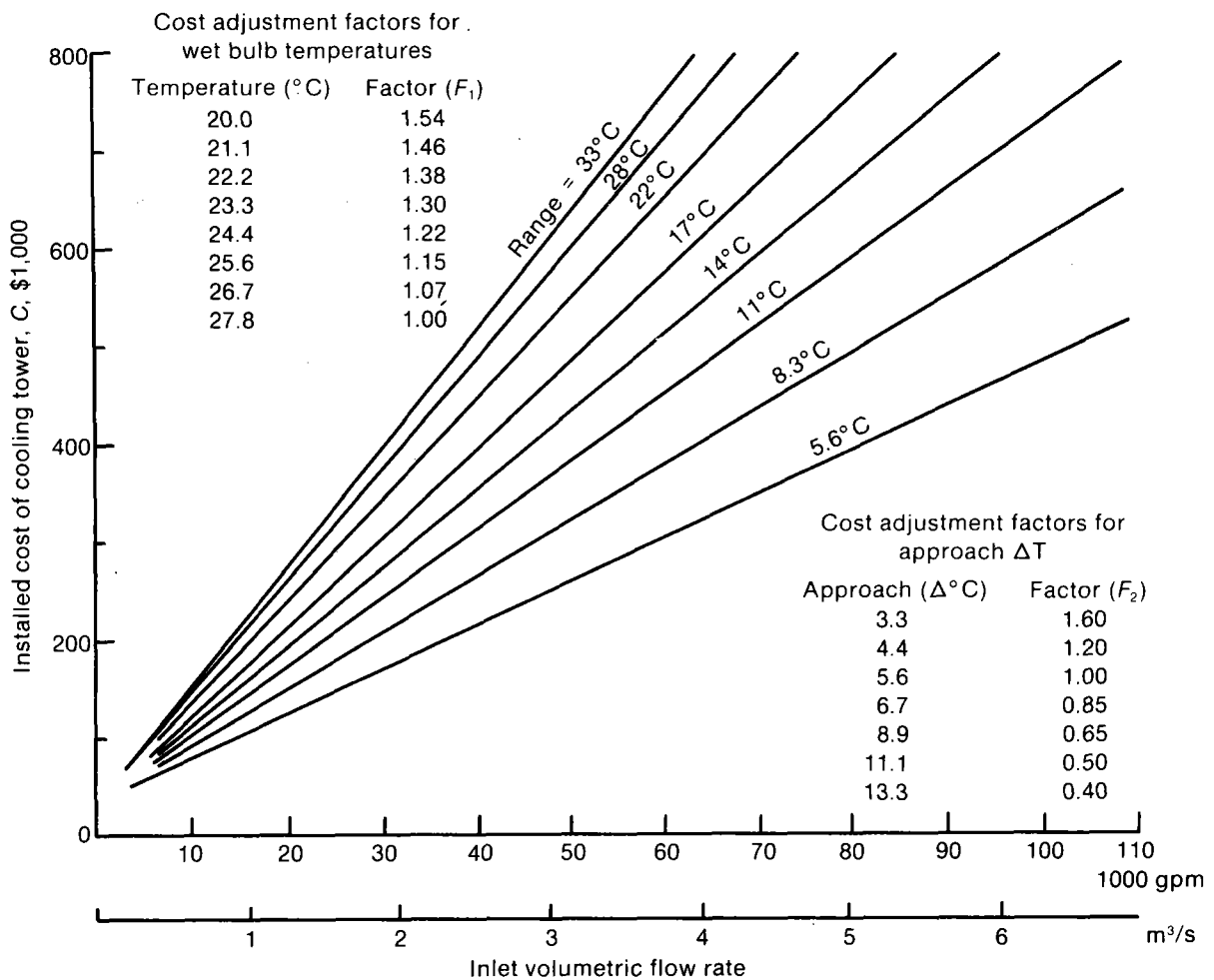
Figure 7-1. Cost of Cooling Towers
Source: Vatavuk and Neveril 1981.

48

available for the operating conditions under consideration, so we used the closest available factors: $F_1 = 1.54$ and $F_2 = 1.6$. The cost, adjusted using the formula recommended by Vatavuk and Neveril $C_{adjusted} = (C - 34,500) F_1 F_2 + 34,500$, becomes \$400,000. Thus, according to the empirical formula for parasitics, the fans will use 198.8 kW of electricity.

The other contribution of the coolant tower to parasitics is the water's headloss in falling the height of the tower (3.5 m). This nonrecoverable loss contributes 72.4 kW to the parasitics.

7.2 PLANT EFFICIENCY

The parasitic losses of the entire plant are itemized in Table 7-1. The losses of the condenser subsystem were computed in Section 7.1, and then divided by the efficiency of the pump, where appropriate, to give the electricity requirements. Throughout this report pumps are assumed to have an efficiency of 80%; compressors, 70%; and the turbine, 90%.

Plant efficiency is calculated from the parasitics listed in Table 7-1 and from the heat absorbed and rejected by the system. In the boiler, the pentane absorbs 50.945 MW_t from the brine. In the condenser, it rejects 44.9305 MW_t. Thus, the work performed by the brine on the turbine is 6.0145 MW. The turbine converts 90% of this to electricity, so the gross power output is 5.413 MW_e. The net work out, obtained by subtracting the parasitic losses from this, is 4.576 MW. This gives an efficiency of 8.98%. The use of a cooling pond rather than a cooling tower would improve the efficiency substantially, as shown in the next section.

Table 7-1. Parasitic Losses

Parts of the Plant	Losses (kW)
Condenser Subsystem	
Frictional headloss in shell-and-tube condenser	237.2
Gravity headloss in cooling tower	90.6
Work of fans in cooling tower	198.8
Subtotal	526.6
The Rest of the Plant	
Work of pumping pentane from condenser to boiler	53.8
Work of pumping brine from pond to boiler	256.4
Subtotal	310.2
Total	836.8

Wright's analysis of the solar pond power plant (1981), concerned mainly with a comparison of boiler systems, neglects the parasitic losses associated with the shell-and-tube condenser system, but these parasitic losses are significant and reduce the output of the plant to 4.58 MW_e. (This is not simply equal to the difference between 5 MW_e and the new parasitics of the condenser system because the assumptions that Wright made in that analysis are different from the ones made in this report. Under the assumptions used in this report, Wright's plant, as designed, would have produced 5.103 MW_e if there were no parasitics in the condenser subsystem.)

7.3 SCALE-UP: SIZING AND COSTING

In order to produce 5 MW_e net, it is necessary to increase the heat input and thus the pentane flow rate over those selected by Wright (1981) by a factor of 5/4.58. So, the pentane mass flow rate of the new system must be 126 kg/s. This affects the size and cost of the condenser subsystem and of the rest of the plant as well, including the solar pond.

The surface area of the shell-and-tube condenser is proportional to the heat that must be rejected and thus to the mass flow rate. So the tube surface area for the enlarged condenser is approximately 12,000 m^2. The cost of large heat exchangers is essentially proportional to the heat transfer surface area. Stearns-Roger (Dubberly et al. 1981) provides a cost estimate in 1980 dollars for carbon-steel heat exchangers of $215 to $270/$m^2$. At $215/$m^2$, the shell-and-tube condenser should cost $2,580,000.

The cooling tower must be costed again using Figure 7-1 and the new coolant flow rate, 2300 kg/s of water. The adjusted cost is C_a = ($196,000 − $34,500) × 1.54 × 1.6 + $34,500, or $433,000 in 1977 dollars. In 1980 dollars, the cooling tower costs $565,000. The cooling tower cost includes the cost of pumps, motors, and fans. However, it does not include the cost of a pump to overcome the pressure drop in the condenser. This pump will cost approximately $28,800. The costs of the subsystem components are listed in Table 7-2.

Table 7-2. Cost of Shell-and-Tube Condenser Subsystem

Component	Cost ($K)
Condenser	2,580.0
Pumps	28.8
Cooling tower	433.0
Total	3,041.8

The cost of the shell-and-tube condenser subsystem could be reduced significantly if the cooling tower could be replaced by a cooling pond. This would reduce parasitics. The plant's efficiency would be 9.55%, and the flow rates would have to be increased from Wright's design by a factor of only 5/4.87. This implies a condenser cost of $2,430,000.

SECTION 8.0

SCALE-UP AND COSTING OF THE REST OF THE PLANT

In the preceding two sections, the cost of the four condenser subsystem options are estimated for plants producing 5 MW_e net. This section provides cost estimates for the solar pond and the rest of the plant, scaled up to produce 5 MW_e with each of the condenser subsystems. The first subsection outlines the scale-up procedure, and the second one applies this procedure to the plant and the solar pond.

8.1 SCALE-UP METHOD

The cost of the power plant, excluding the condenser subsystem, is estimated by the ratio method. It is assumed to be proportional to plant capacity (or pentane flow rate) to the six-tenths power. The first column in Table 8-1 shows Wright's estimate (1981) of the cost of an entire organic Rankine cycle power plant with direct-contact boiler and shell-and-tube condenser in 1980 dollars. The estimate was derived by scaling up an estimate by Daedalean Associates for a 0.8 MW_e plant (Weinreich 1980). The scaled-up version has a pentane flow rate of 115 kg/s and was designed to produce 5 MW_e. However, that design neglected parasitic losses in the condenser subsystem, which would be considerable, and so the plant would produce only 4.58 MW_e as designed.

The first ten items in the list are estimates of the FOB costs of major pieces of equipment and of support structures and equipment. The sum of these, a labor charge, and the indirect cost (temporary facilities, construction equipment, project accounting, etc.), is the total field cost. Fees for engineering, contingency, escalation, owner costs, and AFDC are added to the field cost to give the total capital cost. Engineering service refers to the cost of the detailed design and construction supervision provided by the engineering firm that builds the power plant. The contingency factor is an estimate of the investment required to compensate for weather-related problems, strikes, small design changes, estimation errors, and other unforeseen costs. Escalation is a factor in accounting for price increases due to inflation during construction. Owner costs are the expenses incurred by the utility in overseeing construction and licensing the plant for start-up. AFDC (allowance for funds during construction) is the interest paid on the money used to construct the power plant. Each of these fees is a percentage of the preceding total.

The second column in Table 8-1 shows a revision of Wright's estimate, omitting the plant components in the condenser subsystem. The cost of the cooling system and half the cost of the pumps is omitted, and the cost of the direct-contact boiler is replaced by a cost estimate from Wright's more recent report (1982) for a packed-bed direct-contact boiler. The total field cost of this column is multiplied by a scaling factor for each of the four plant designs. Then the cost of the condenser subsystem, estimated in Sections 6.3 and 7.3, is added, and the capital cost is computed from this sum using the method employed in the first column.

Table 8-1. Capital Costs of Organic Rankine Cycle Power Plant ($K)

	Wright's Estimate	Revised Version, excluding Condenser Subsystem
Direct-contact boiler	156	138
Cooling system (shell-and-tube condenser/ evaporative cooling tower)	1,800	--
Turbine (axial)	200	200
Control system	285	285
Valves and piping	765	765
Pumps	251	126
Other mechanical equipment	135	135
Electrical	225	225
Civil works	250	250
Miscellaneous hardware	440	440
Labor	1,200	1,200
Direct field cost	5,708	3,764
Indirect cost	600	600
Total field cost	6,308	4,364
Engineering service (12%)	763	
	7,071	
Contingency (20%)	1,414	
Total construction cost	8,485	
Escalation (7%)	594	
	9,079	
Owner's cost (8%)	726	
	9,805	
AFDC (12%)	1,177	
Total Capital Cost	10,981	

The other capital costs associated with producing power in this way are the cost of the solar pond and, for direct-contact heat exchangers, the cost of pentane lost to the atmosphere. The solar pond size and cost are assumed to be linearly dependent on the amount of heat transferred to the working fluid in the boiler, and thus to the mass flow rate of the working fluid. The cost of lost pentane, treated as an operating expense in Wright's 1981 report, can be converted to a capital expense as follows: assuming a plant-life of 30 years, a fixed-charge rate of 17%, and an annual escalation rate of 7%, the present worth of a system can be obtained by multiplying total capital costs by a factor of 1.6 and operating costs by a factor of 20.1 (Dubberly et al. 1981). If all costs are to be compared on the basis of capital costs, as in this analysis, operating costs must be multiplied by a factor of 20.1/1.6, or 12.56. The only operating cost that enters into our comparison is the cost of replacing lost pentane.

8.2 SCALE-UP OF PLANT AND SOLAR POND

Table 8-2 summarizes the scaled-up costs of power plant and solar pond. In this section, we describe how these figures are derived for the drop-type condenser plant, as an example.

8.2.1 Plant Costs

According to the "six-tenths rule" (Peters and Timmerhaus 1968), the cost of a plant is roughly proportional to its capacity, raised to the six-tenths power. We assumed that the capacity of each of these plants is proportional to the working fluid mass flow rate, and thus to net power output. So, in order to enlarge the drop-type condenser plant described in Table 8-2 (which produces 4.29 MW_e) to produce 5 MW_e, the plant cost should be multiplied by a scale-up factor of $(5/4.29)^{0.6}$, or 1.096. Since the condenser subsystem for the enlarged plant is costed separately in Section 6.3.1, this factor is applied to the field cost of the rest of the plant ($4,364,000), giving $4,781,000. To this is added the cost of the condenser subsystem from

Table 8-2. Scaled-Up Costs of Power Plant and Solar Pond

	Type of Condenser			
	Drop-Type	Bubble-Type	Packed-Bed	Shell-and-Tube
Scale-up factor for plant	1.096	1.058	1.071	1.055
Total field cost of plant excluding condenser subsystem	4,781	4,617	4,676	4,602
F.O.B. cost of condenser subsystem	2,626	2,091	2,286	3,042
Total field cost of plant	7,408	6,708	6,962	7,644
Total capital cost of plant	12,898	11,669	12,121	13,309
Total capital cost of pond	14,833	13,982	14,290	13,916
Capital cost of pentane replacement	52	49	50	3
Total Capital Cost	27,783	25,700	26,461	27,228
Capital cost per kW_e	5.557	5.14	5.292	5.446
Plant efficiency	8.43%	8.94%	8.75%	8.98%
Brine flow rate (kg/s)	3,116	2,939	3,002	2,300[a]
Pentane flow rate (kg/s)	134	126	129	126

All costs are in 1980 $K.

[a]Fresh water.

Table 6-4, $2,626,500. The sum of these costs, $7,408,000, is the total field cost of the plant. With the addition of engineering and contingency fees, escalation, owners cost, and AFDC, the total capital cost of the plant is $12,898,000.

8.2.2 Solar Pond Costs

For large solar ponds, it is reasonable to assume that heat extracted and pond cost are proportional to pond area. If the year-round average incident solar radiation on the pond is 250 W/m^2, and 16% of this amount is stored in the pond, then energy can be extracted from the pond at a rate of 40 W/m^2. (The 16% conversion efficiency is an extrapolation from the performance of small ponds to large ponds, for which losses of energy to the ground should be small.) Cost estimates for solar ponds vary from $5/m^2$ to $18/m^2$, depending on whether a liner is used, how much construction work is required, and how large the pond is (Jet Propulsion Laboratory 1982; May et al. 1982). We chose an intermediate value, $10/m^2$, for our calculations.

The cost of the solar pond for the drop-type condenser plant is calculated as follows: first, the required rate of heat removal from the pond is computed. Since this power plant operates at an efficiency of 8.43% and produces 5 MW_e of power, it must absorb 5 MW_e/0.0843, or 59.3 MW_t from the pond. This determines the pond area, 59.3 $\times$ 10^6 W $\div$ 40 W/m^2 = 1.483 $\times$ 10^6 m^2. At $10 per square meter, the pond costs $14,833,000.

8.2.3 Pentane Loss Costs

The loss of pentane to the atmosphere is proportional to the brine flow rate and the concentration of pentane in the brine as it leaves the degasser. For all of the direct-contact designs, the exit concentration of pentane in brine is 0.0818 ppm (by weight). For the drop-type condenser subsystem with a brine flow rate of 3116 kg/s, the pentane loss is 22.0 kg/day, or 8000 kg/year. (We assume that all the pentane dissolved in the brine of the evaporating pond is desorbed into the air.) If pentane costs $0.49/kg (Chemical Marketing Reporter, quoted by Wright 1981), then the cost per year for pentane replacement is $3,900. To this must be added the cost of replacing the pentane lost through the direct-contact boiler, $200/year, according to Wright's loss rate calculations (1981). The capitalized cost of this operating expense is $4100 $\times$ 20.1/1.6 = $52,000. From the point of view of plant cost, obviously it would be advantageous to lose more pentane and reduce the size of the degasser. However, the upper limit on the loss rate is set by the safety constraints described in Section 3.0.

SECTION 9.0

CONCLUSIONS

The purpose of this report is to determine whether a direct-contact condenser is a feasible replacement for the conventional shell-and-tube condenser for a 5 MW$_e$ solar pond power plant. Three direct-contact design options are compared to the shell-and-tube condenser. Sizing and costing are performed in Sections 6.0 through 8.0, and final cost results are presented in Tables 6-4, 7-2, and 8-2. Table 8-2 shows that some of the power plants using direct-contact condensation cost less then the plant with the shell-and-tube condenser, by as much as 5%. The condenser subsystem price was reduced by as much as 30%, but the rest of the system was more expensive because of its reduced efficiency. Moreover, because the uncertainty associated with the design is far less for shell-and-tube condensers than for direct-contact condensers, the shell-and-tube option would probably be preferable unless the direct-contact condenser subsystem were less expensive by at least 50%. So, the direct-contact condenser subsystems, as designed, are not inexpensive enough to justify the risks inherent in a relatively new technology.

It is important to note that the deaerator and degasser, not the condenser itself, account for the major part of the cost of the direct-contact condenser subsystem. The deaerator and degasser contribute between 63% and 75% to the cost of the condenser subsystem, and are responsible for between 68% and 99% of the subsystem's parasitic losses. (The parasitic losses caused by pipe friction and the work of the compressors associated with the vent condenser are neglected. The figure of 99%, calculated for the bubble-type condenser, may be unrealistically high.) Thus, the plant's efficiency would be increased significantly if the degasser and deaerator could be eliminated. There may be types of deaerators and degassers that are less expensive and have smaller parasitic losses than the packed-bed design that we have considered here. A literature search of degasser and deaerator designs and an evaluation of commercially available equipment might uncover a better design, which could change the cost of direct-contact options drastically.

In order to understand the possible impact on plant cost of smaller deaerators and degassers, we made a cost estimate of a plant with a bubble-type condenser and no deaerator or degasser. The cost of the condenser subsystem was reduced to approximately 20% of the cost of the shell-and-tube subsystem; the cost of the rest of the system was also reduced because of higher efficiency. The final cost was approximately 20% of the cost of the shell-and-tube plant.

Another major area of uncertainty lies in particle spacing and multiparticle effects in the bubble-type and drop-type condensers. The choice of bubble and spray-nozzle spacing was arbitrary. The effect of changing this spacing can be seen from Table 6-4. The cost of the condenser is roughly proportional to cross-sectional area, and parasitic losses are independent of area. Thus, changing spacing will affect the cost of the condenser, but not of the other components or the pond and the rest of the plant. Since the condenser cost is outweighed by the combined cost of deaerator and degasser, a moderate change in spacing is unlikely to change the conclusions of this report.

Even if the use of a direct-contact condenser with deaerator and degasser is not competitive, there are other possible subsystems using a direct-contact condenser. Figure 9-1 shows two of these possibilities along with (a) the shell-and-tube subsystem and (b) the direct-contact subsystem considered in this report. Option (a), the shell-and-tube subsystem, consists of a shell-and-tube condenser and a wet cooling tower, which is a direct-contact air-water heat exchanger. Option (b) includes two direct-contact heat exchangers: the condenser and the evaporating pond. The deaerator and degasser are necessary to reduce contamination with air of the working fluid and loss of working fluid to the air.

Option (c) was designed to remove the possibility of working fluid contamination and loss, and thus the need for the deaerator and degasser. Pentane vapor condenses by direct contact with water, which is cooled in a shell-and-tube, liquid-liquid heat exchanger. Thus, the water never comes into contact with the atmosphere, and can neither desorb pentane nor absorb air. The water traveling through the other side of the liquid-liquid heat exchanger is exposed to air in the cooling tower. So, the secondary heat exchanger separates the working fluid loop from the air, allowing heat transfer but no mass transfer. This subsystem is of interest only if the combined cost of the direct-contact condenser and the shell-and-tube, liquid-liquid heat exchanger is smaller than the cost of a shell-and-tube condenser that performs the same function for the same overall temperature difference between air and pentane, i.e., if it compares favorably with option (a). We examined this possibility briefly and found that the shell-and-tube, liquid-liquid heat exchanger has a higher overall heat transfer coefficient U_s, than the shell-and-tube condenser. However, it must operate over a smaller temperature difference than the condenser option (a). In the subsystem of option (c), the pentane-air temperature difference is split between two heat exchangers. This more than compensates for the enhanced heat transfer coefficient. The area required for the liquid-liquid heat exchanger, which is inversely proportional to $U_s\Delta T$, is greater than that required for the shell-and-tube condenser of option (a). Thus, even neglecting the cost of the direct-contact condenser, option (c) is more expensive than the conventional option (a).

The final possibility, option (d), is not analyzed in this study, and may merit further consideration. It consists of a direct-contact condenser and a dry cooling tower, which is not a direct-contact device. In the cooling tower, water travels through finned tubes. Heat transfer can be further enhanced by spraying water on the outside of the tubes. As in options (a) and (c), there is no problem of working-fluid loss or contamination. However, it seems unlikely that this design will result in a substantial cost reduction over option (a). Option (a) is expensive because the condenser must have a very large metal heat transfer surface. In option (d), the cost of the condenser will be reduced because of direct contact between the coolant and condensing vapor, but a large expensive metal surface will be required in the cooling tower.

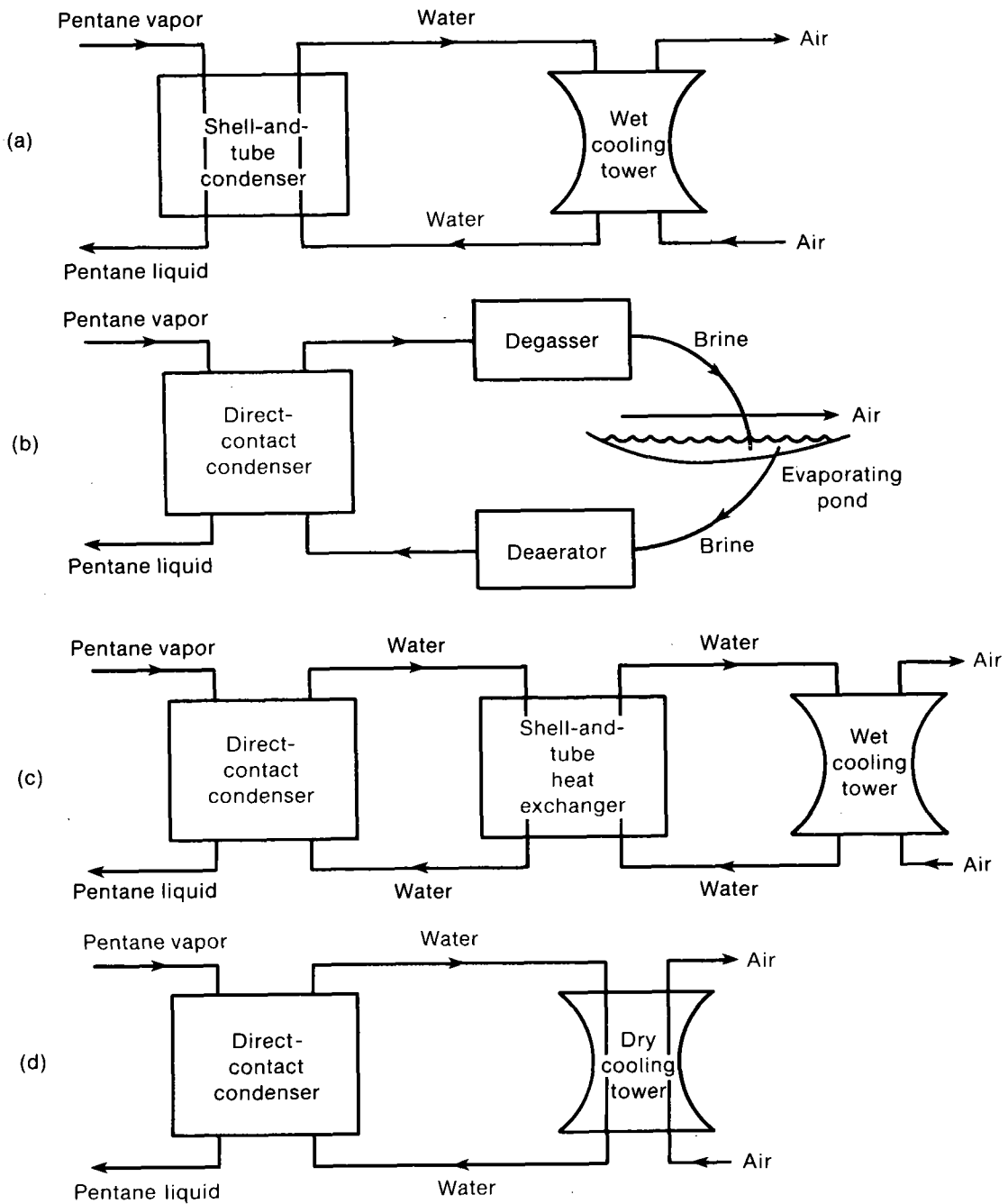**Figure 9-1. Condenser Subsystem Options**

SECTION 10.0

REFERENCES

Clift, R., J. R. Grace, and M. E. Weber. 1978, Bubbles, Drops, and Particles, New York, NY: Academic Press, 380 pp.

Diamant, R. M. E., 1971, The Prevention of Corrosion, London: Business Books Limited, 199 pp.

Dubberly, L. J., J. E. Gormely, J. A. Kochman, W. R. Lang, and A. W. McKenzie, 1981 (Dec.), Cost and Performance of Thermal Storage Concepts in Solar Thermal Systems; Phase 2: Liquid Metal Receiver, SERI/TR-XP-0-9001-1-B, Golden, CO: Stearns-Roger Services, Inc., for Solar Energy Research Institute.

Golshani, A., and F. C. Chen, 1981 (Sept.), Ocean Thermal Gas Desorption Studies, ORNL/TM-7438/V2, Oak Ridge, TN: Oak Ridge National Laboratory, available from NTIS, Springfield, VA 22161.

Guthrie, K. M., 1969 (Mar. 24), "Data and Techniques for Preliminary Cost Estimating," Chemical Engineering, pp. 114-142.

Hellstrom, George W., Harold R. Jacobs, and Robert F. Boehm, 1976 (Dec.), The Solubility of Selected Secondary Fluids for Use in Direct-Contact Geothermal Power Cycles, IDO/1549-6, Salt Lake City, UT: University of Utah, available from NTIS, Springfield, VA 22161.

Isenberg, Jerrold, David Moalem, and Samuel Sideman, 1970, "Direct-Contact Heat Transfer with Change of Phase: Bubble Collapse with Translatory Motion in Single and Two Component Systems," Proceedings of the 4th International Heat Transfer Conference, Paris, 1970, Vol. 5, paper B2.5.

Jacobs, Harold R., 1984, "Direct-Contact Condensers," in Heat Exchanger Design Handbook, New York, NY: Hemisphere Press (in press).

Jacobs, H. R., Jeff A. Bogart, and Ralph W. Pensel, 1982, "Condensation on a Thin Film Flowing Over an Adiabatic Sphere," Proceedings of the 7th International Heat Transfer Conference, Munich, 1982, Vol. 5, pp. 89-94.

Jacobs, Harold R., and Donald S. Cook, 1978, "Direct-Contact Condensation on a Noncirculating Drop," Proceedings of the 6th International Heat Transfer Conference, Toronto, 1978, Vol. 2, pp. 389-393.

Jacobs, H. R., Heimir Fannar, and George C. Beggs, 1978, "Collapse of a Bubble of Vapor in an Immiscible Liquid," Proceedings of the 6th International Heat Transfer Conference, Toronto, 1978, Vol. 2, pp. 383-387.

Jacobs, H. R., and B. H. Major, 1982, "The Effect of Noncondensible Gases on Bubble Condensation in an Immiscible Liquid," Transactions of the ASME, Vol. 194, pp. 487-492.

Jacobs, H. R., K. D. Thomas, and R. F. Boehm, 1979, "Direct-Contact Condensation of Immiscible Fluids in Packed Beds," Proceedings of the 18th Natinal Heat Transfer Conference, San Diego, CA: 6-8 Aug. 1979, New York, NY: American Society of Mechanical Engineers, pp. 103-110.

Jet Propulsion Laboratory, 1982 (Mar. 15), Regional Applicability and Potential of Salt-Gradient Solar Ponds in the United States, DOE/JPL 1060-50, Vol. 2, JPL Publication 82-10, Vol. 2, Pasadena, CA: JPL.

M. W. Kellogg Company, 1975 (Oct.), Saline Water Conversion Engineering Data Book--1975, Office of Water Research and Technology, Department of the Interior, PB-250 907, available from NTIS, Springfield, VA 22161.

May, E. Kenneth, Cécile M. Leboeuf, and David Waddington, 1982 (Dec.), Conceptual Design of the Truscott Brine Lake Solar Pond System, SERI/TR-253-1833, Golden, CO: Solar Energy Research Institute, available from NTIS, Springfield, VA 22161.

Mersmann, Alfons, 1978, "Design and Scale-up of Bubble and Spray Columns," Ger. Chem. Eng., Vol. 1, pp. 1-11.

Perry, Robert H., and Cecil H. Chilton, (1973), Chemical Engineers Handbook, 5th edition, New York: McGraw-Hill.

Peters, Max S., and Klaus D. Timmerhaus, 1968, Plant Design and Economics for Chemical Engineers, New York, NY: McGraw-Hill, 850 pp.

Pikulik, A., and H. Diaz, 1977 (Oct. 10), "Cost Estimating for Major Process Equipment," Chemical Engineering, pp. 106-122.

Robertson, R. C., 1980 (Mar.), "Condensers," Sourcebook on the Production of Electricity from Geothermal Energy, edited by Joseph Kestin, DOE/RA/28320-2, Providence, RI: Brown University; available from U.S. Government Printing Office, Washington, DC 20585.

Sax, N. Irving, 1979, Dangerous Properties of Industrial Materials, 5th edition, New York, NY: Van Nostrand Reinhold Co, 1118 pp.

Schumacher, M., editor, 1979, Seawater Corrosion Handbook, Park Ridge, NJ: Noyes Data Corporation, 493 pp.

Sideman, Samuel, and David Moalem-Maron, 1982, "Direct-Contact Condensation," Advances in Heat Transfer, Vol. 15, pp. 227-281.

Smith, P. L., and Matthew Van Winkle, 1958 (Sept.), "Discharge Coefficients through Perforated Plates at Reynolds Numbers of 400 to 3000," A.I.Ch.E. Journal, Vol. 4 (No. 3), pp. 266-268.

Vatavuk, William M., and Robert B. Neveril, 1981 (Mar. 23), "Cost File Part VI: Estimating Costs of Dust-Removal and Water-Handling Equipment," Chemical Engineering, pp. 222-228.

Weinreich, R. S., and F. J. Franz, 1980 (July), The Research and Development of a 3000 GPM Power Plant for the Design, Development, and Demonstration of a 100 kW Power System Utilizing the Direct Contact Heat Exchanger Concept for Geothermal Brine Energy Recovery (GEOBER) Program, DAI Technical Report FJF-7802-001-TR, Woodbine, MD 21797: Daedalean Associates, Inc.

Wright, J. D., 1981 (June), (revised June 1982), An Organic Rankine Cycle Coupled to a Solar Pond by Direct-Contact Heat Exchange—Selection of a Working Fluid, SERI/TR-631-1122R, Golden, CO: Solar Energy Research Institute; available from NTIS, Springfield, VA 22161.

Wright, J. D., 1982 (May), Sizing of Direct-Contact Preheater/Boilers for Solar Pond Power Plants, SERI/TR-252-1401, Golden, CO: Solar Energy Research Institute; available from NTIS, Springfield, VA 22161.

DISTRIBUTION

Bill Banks
Tulsa District
U.S. Army Corps of Engineers
P.O. Box 61
Tulsa, OK   74121

John Bigger
Electric Power Research Institute
3412 Hillview Ave.
Palo Alto, CA   94304

Bill Boegli
Bureau of Reclamation
U.S. Department of the Interior
P.O. Box 25007
Building 67
Denver Federal Center
Denver, CO   80225

Robert Boehm
Department of Mechanical and
   Industrial Engineering
University of Utah
Salt Lake City, UT   84117

Robert L. French
Jet Propulsion Laboratory
4800 Oak Grove Drive
Pasadena, CA   90041

Donald Harleman
Ralph M. Parsons Laboratory
Department of Civil Engineering
Massachusetts Institute of
   Technology
Cambridge, MA   02139

Stanley J. Hightower, Coordinator
Advanced Energy Applications
Bureau of Reclamation
U.S. Department of the Interior
P.O. Box 25007
Building 67
Denver Federal Center
Denver, CO   80225

Harold R. Jacobs
Department of Mechanical and
   Industrial Engineering
University of Utah
Salt Lake City, UT   84117

Benjamin M. Johnson
Pacific Northwest Laboratory
Battelle Memorial Institute
Richland, WA   99352

J. L. Matthews
Tulsa District
U.S. Army Corps of Engineers
P.O. Box 61
Tulsa, OK   74121

Igal Meitlis
Salton Sea Project
Southern California Edison Company
P.O. Box 800
Rosemead, CA   91770

Fred Morse
U.S. Department of Energy
1000 Independence Ave.
Washington, DC   20585

Lyn J. Rasband
Utah Power and Light Company
1407 West No. Temple St.
P. O. Box 899
Salt Lake City, UT   84110

Harry Remmers
Advanced Energy Applications
Bureau of Reclamation
U.S. Department of the Interior
P. O. Box 25007
Building 67
Denver Federal Center
Denver, CO   80225

Steve Sargent
SERI Site Office
U.S. Department of Energy
1617 Cole Boulevard
Golden, CO   80401

Sam Schweitzer
Division of Solar Thermal Technology
U.S. Department of Energy
1000 Independence Ave.
Washington, DC   20585

SERI ⬤ ——————————————————————————

Graham Siegel
Tennessee Valley Authority
1850 Commerce Union Bank Building
Chattanooga, TN 37401

Tex Wilkins
U.S. Department of Energy
1000 Independence Ave.
Washington, DC 20585

4. Title and Subtitle		5. Publication Date
Direct-Contact Condensers for Solar Pond Power Production		May 1984
		6

7. Author(s) Elizabeth M. Fisher, John D. Wright	8. Performing Organization Rept. No.

9. Performing Organization Name and Address	10. Project/Task/Work Unit No. 4406.10
Solar Energy Research Institute 1617 Cole Boulevard Golden, Colorado 80401	11. Contract (C) or Grant (G) No. (C) (G)

12. Sponsoring Organization Name and Address	13. Type of Report & Period Covered Technical Report
	14.

15. Supplementary Notes

16. Abstract (Limit: 200 words)

The use of a direct-contact condenser as a way of reducing the cost of electricity from an organic Rankine cycle power plant coupled to a solar pond is examined. Three possible direct-contact heat exchangers are considered: drop-type, bubble-type, and packed-bed. Each condenser is designed to operate with a deaerator and a degasser to reduce contamination and loss of working fluid. Appropriate correlations and models from the literature for heat and mass transfer, particle terminal velocity, and particle production are presented. Each piece of equipment is sized and costed. Finally, the cost of the entire power plant is compared with that of a plant using a conventional shell-and-tube condenser. For two of the three direct-contact designs, a reduction in the cost of electricity is estimated. However, the reduction is not significant enough to compensate for the uncertainties involved in the relatively new technology of direct-contact heat transfer.

17. Document Analysis

a. Descriptors Brines ; Condensers ; Design ; Heat Transfer ; Pentane ; Rankine Cycle ; Rankine Cycle Power Systems ; Solar Ponds ; Solar Thermal Power Plants

b. Identifiers/Open-Ended Terms

c. UC Categories

62e

18. Availability Statement	19. No. of Pages
National Technical Information Service U.S. Department of Commerce 5285 Port Royal Road Springfield, Virginia 22161	75
	20. Price A04

UNITED STATES DEPARTMENT OF ENERGY
P.O. BOX 62
OAK RIDGE, TENNESSEE 37830

OFFICIAL BUSINESS
PENALTY FOR PRIVATE USE. $300

POSTAGE AND FEES PAID

UNITED STATES
DEPARTMENT OF ENERGY

U S MAIL

```
          12699            FS-  1
SANDIA NATIONAL LABORATORIES
ATTN  THOMAS BRUMLEVE
LIVERMORE, CA       94550
```